Primary Cilia Directionality Reveals a Slow Reverse Movement of Principal Neurons for Postnatal Positioning and Lamina Refinement in the Cerebral Cortex

Juan Yang[1,2], Soheila Mirhosseiniardakani[1,3], Liyan Qiu[1], Kostandina Bicja[1], Abigail Del Greco[1], Kevin Jungkai Lin[1], Mark Lyon[4], and Xuanmao Chen[1,*]

[1]Department of Molecular, Cellular, and Biomedical Sciences; Graduate Programs in [2]Biochemistry and [3]Genetics; College of Life Sciences and Agriculture, University of New Hampshire, Durham, NH 03824.

[4]Department of Mathematics and Statistics, College of Engineering and Physical Sciences, University of New Hampshire, Durham, NH 03824

[*] Correspondence should be addressed to Dr. Xuanmao Chen: Department of Molecular, Cellular, and Biomedical Sciences, College of Life Sciences and Agriculture, University of New Hampshire, Rudman Hall Rm 389, 46 College Road, Durham, NH 03824. Phone: 603 862 4542, Fax: 603 862 4013, Email: Xuanmao.Chen@unh.edu.

Running Title: Cilia Orientation Indicates Principal Neuron Positioning

Key Words: Neuronal Primary Cilia, Principal Neuron Positioning, Cortical Lamination, Reverse Movement, Ift88 and Arl13b

Acknowledgments: This study was supported by National Institutes of Health Grants K01AG054729, P20GM113131-7006, R15MH126317, and R15MH125305 to X.C.; UNH CoRE PRP awards and Cole Neuroscience and Behavioral Faculty Research Awards to X.C.; UNH Summer TA Research Fellowships (STAF) and a Dissertation Year Fellowship (DYF) to J.Y. We would like to thank Brendon Lewis for helping analyze cilia directionality in the ventral CA1 region. We are grateful to the University Instrumentation Center at UNH for A1R HD confocal imaging service.

Abstract

Currently little is known about neuronal positioning and the roles of neuronal primary cilia in postnatal neurodevelopment. Here we show that primary cilia of principal neurons do not fully arise until the postnatal stage, and they undergo marked changes in positioning and orientation, concurrent with postnatal principal neuron positioning and maturation in the mouse cerebral cortex. Primary cilia of early- and late-born CA1 principal neurons display opposite orientations, while primary cilia of principal neurons in the subiculum, entorhinal cortex, and neocortex largely point in the direction of the pia. In contrast, astrocytes and interneurons in the hippocampus, and neurons in nucleated brain regions do not display specific cilia directionality. Guided by the clue of cilia directionality, we discovered that the cell bodies of principal neurons in the hippocampal CA1 superficial sublayer, subiculum, postsubiculum, and neocortex undergo a previously unnoticed, slow but substantial "reverse movement" for postnatal positioning and lamina refinement. Further, selective disruption of cilia function in the forebrain using Ift88 conditional knockout mice leads to cortical expansion, altered cortical lamination, or gyrification in the retrosplenial cortex that is formed through a reverse movement. Collectively, this work has identified reverse movement as a fundamental process for principal cell positioning that refines lamination in the cerebral cortex and may impact the cortical evolution of mammals.

Introduction

Neuronal primary cilia are microtubule-based surface projections, which are widely expressed throughout the central nervous system [1-3]. They regulate various physiological functions including neurodevelopment, energy balance, and cognitive function [3-6]. Defects in primary cilia are associated with a variety of disorders including neurodevelopmental disorders, obesity, and cognitive impairment [3, 7, 8]. It is known that primary cilia modulate embryonic neurodevelopment [8, 9] by influencing cell fate specification in the ventral neural tube [10, 11] or forebrain neuronal patterning by regulating radial glia cell polarity [12-14]. Evidence also implicates primary cilia in neural circuit formation in the adult brain by forming atypical axon-cilium synapses [15] and hippocampal memory by affecting adult neurogenesis [8, 16, 17]. However, the roles of neuronal primary cilia in postnatal neurodevelopment are poorly understood.

Principal neurons in the cerebral cortex migrate from the germinal zone to their destinations for placement via multiple steps [18-20]. One crucial step is the radial migration crawling along radial glial fibers and moving towards the pia [21]. The nuclear translocation of radial migration occurs in a saltatory manner, in which the centriole moves forward in the leading process, followed by nuclear translocation [22-24]. The centriole is connected to the nucleus through microtubule network. Hence, the movements of the centriole and nucleus are tightly coupled. Pyramidal neurons in the mammalian cerebral cortex are organized into highly laminated structures, which are subdivided into the deep and superficial sublayers along the radial axis [25, 26]. These two sublayers harbor early- and late-born principal neurons, respectively, which migrate to the hippocampal or cortical plate in a birthtime-dependent inside-out pattern [26, 27]. Following the radial migration that occurs primarily during embryonic stage [28, 29], Pyramidal neurons undergo positioning and subsequently become matured to develop synaptic connectivity [30, 31]. The first two weeks after birth are the critical period for neuronal positioning and maturation in the mouse cerebral cortex, when the hippocampal superficial and deep sublayers gradually condense into the compact stratum pyramidale (SP) [32], whereas the neocortical principal cell layer

expands drastically to form five sparse laminae (Layer II-VI) [33]. Although numerous studies have contributed to uncovering the cellular and molecular mechanisms of radial migration during embryonic development, it is not well understood how pyramidal neurons in the cerebral cortex complete positioning during early postnatal development.

Given the centriole generally directs where the nucleus of a central neuron is placed, primary cilia after emanating from the centrioles may indicate the positioning process of principal neurons in the cerebral cortex, and ciliation timing and cilia directionality provides useful clues. Thus, we performed cilia morphology and directionality analyses in the postnatal mouse cerebral cortex. We first observed that primary cilia of projection neurons in the cerebral cortex do not fully arise until the postnatal stage. Intriguingly, primary cilia of early- and late-born hippocampal neurons display opposite directionality, while cilia of both early- and late-born neocortical neurons generally point toward the pia direction. This clue gradually led us to discover that principal neurons in many cerebral cortical sub-regions, including the hippocampal CA1 superficial sublayer, subiculum, postsubiculum, and neocortex, are subject to a slow but substantial reverse movement. This reverse movement refines the configuration of various cortical laminae spanning from the neocortex to the hippocampal CA1 region. We further found that selective ablation or shortening of primary cilia in the forebrain using Ift88 floxed mice [34-36] causes cortical expansion, altered cortical laminae, or gyrification in the retrosplenial cortex that is formed via an invagination driven by the reverse movement of principal neurons. Shortening cilia using Arl13b floxed mice [37] yield similar results. Together, we identified a slow but substantial “reverse movement” of principal neurons for positioning. We propose that the reverse movement of principal neurons is a fundamental process for neuronal placement, pivotal not only for the development of the cerebral cortex, but also in evolutionary transition from the 3-layered compact allocortices to the 6-layered sparse neocortices.

Results

Primary Cilia of Early- and Late-born Hippocampal CA1 Neurons Display Opposite Orientations. To examine the morphological changes of neuronal primary cilia in CA1 SP during postnatal development, we performed immunofluorescence staining on WT brain sections using AC3 [1, 38-40] and Arl13b antibodies [2, 41]. We found that primary cilia morphology and orientation in SP underwent marked changes during early postnatal development (Fig. 1A-D). At postnatal day 5 (P5) and P7, AC3- or Arl13b-marked primary cilia were rarely detected in CA1 SP (Fig. 1A). At P9, many neuronal primary cilia became visible but still very short, and at P10, neuronal primary cilia were markedly elongated, with many clustered at the edge of SP and stratum radiatum (SR) (Fig. 1D). Apparently, these primary cilia exhibited opposite orientations: the axoneme of primary cilia in the superficial sublayer mostly pointed in the SR direction, whereas those in the deep sublayer oriented towards the stratum oriens (SO). Interestingly, from P10 to P14, cilia orientation underwent a drastic change (Fig. 1D). At P10, ~ 40% of cilia orientated toward SO, while at P14 only ~20% of cilia pointed in the SO direction (Fig. 1A-E). At P14, SR-pointing primary cilia occupied most of SP space. SO-pointing primary cilia were then squeezed to the edge at the top. Afterwards at P40 and P75, cilia orientation did not change much, except for becoming less uniformly aligned with the radial axis (Fig. 1A-E). Polar plots and histograms present changes in cilia orientation from P10 to P75 (Fig. 1C). Simultaneously, the thickness of SP decreased significantly from ~95 μm at P3 to ~60 μm at P40 (Fig. 1F) and continued to decrease with age (Fig. S1). This data suggests that CA1 pyramidal neurons continue to adjust their position postnatally, which condenses cell density when some neurons die [42] and decrease SP thickness.

To confirm if primary cilia with opposite orientations come from early- and late-born pyramidal neurons, respectively, we performed immunofluorescence staining using calbindin antibody, a marker for late-born neurons in the hippocampal CA1 after P20 [26, 43]. Primary cilia of calbindin-positive neurons in the superficial sublayer largely pointed in the SR direction, whereas calbindin-negative neurons' primary cilia generally are SO-pointing (Fig. 1G). This data demonstrates that primary cilia of early- and

late-born pyramidal neurons exhibit opposite orientation, suggesting a role of primary cilia in regulating pyramidal cell positioning.

Arl13b Strongly Regulates Neuronal Ciliation in the Hippocampal CA1 Region.

Arl13b is an atypical ciliary small GTPase that modulates ciliogenesis, interneuron placement and maturation [14, 44, 45]. We have previously shown that Arl13b over-expression transgenic mice (Arl13b+) had much longer neuronal primary cilia [41]. We also found that neuronal primary cilia in both WT and Arl13b+ mice were the longest in the hippocampal CA1 region, compared to many other brain regions including CA3, dentate gyrus, neocortex, and amygdala (Fig. S2). We further observed that the expression of AC3 in pyramidal neurons in CA1 SP remained relatively stable after P10 (Fig. 1A). In contrast, the expression of Arl13b started to emerge at P5 (Fig. 1A). At P10, Arl13b expression reached a peak level, starting decrease at P14 and further fade away at P40, becoming very weak in adulthood (Fig. 1A). Arl13b high expression appeared to coincide with pyramidal cell positioning from ~P5 to P14 [46-49], suggesting a role of Arl13b in neuron positioning.

To determine if Arl13b affects ciliation pattern in CA1 SP, we characterized changes in cilia morphology and orientation during postnatal development using Arl13b+ mice and littermate controls. Firstly, overexpression of Arl13b not only elongated primary cilia, but also affected ciliation timing (Fig. 2A-B). Arl13b+ mice started to express primary cilia in the deep sublayer as early as P3, which were SO-pointing (Fig. S3A). At P7, primary cilia of deep-sublayer neurons of Arl13b+ mice were very long, while primary cilia of superficial-sublayer neurons were not fully emanated, with many remaining dot-shaped at SP bottom (Fig. 2A). Likewise, neuronal primary cilia in the deep sublayer of Arl13b+ were largely SO-pointing, whereas those in the superficial-sublayer clearly had opposite orientation (Fig. 2A-B). Secondly, immunostaining images from P7 to ~P75, histograms and polar plots of cilia orientations indicate that primary cilia in CA1 SP of Arl13b+ mice underwent drastic changes in orientation from P7 to P14 and mild changes from P14 to P75 (Fig. 2C-E). This confirms that the time-window before P14 is crucial for changes in cilia positioning and orientation. Thirdly, overexpression of Arl13b slightly affected

the percentage of primary cilia orientation: at P14 and P40, more primary cilia pointed north in Arl13b+ mice than in WT mice (Fig. 2D-F). We also examined cilia directionality in the ventral CA1. Likewise, primary cilia of early- and late-born neurons in the ventral CA1 of both WT and Arl13b+ mice clearly displayed opposite orientations at P9 (Fig. S4). The SR-pointing cilia orientation became more predominant at P40 than P9 (Fig. S4). Lastly, calbindin immunostaining also verified that primary cilia with opposite orientation were from early- and late-born neurons, respectively (Fig. 2G). This data demonstrates significant changes in cilia positioning and orientation during early postnatal development.

Neuronal Ciliation Coincides with Maturation.

Next, we asked the question if neuronal maturation and ciliation occur at the same time-window. We employed a NeuN antibody, a marker for matured pyramidal neurons [50, 51], in an immunofluorescence staining assay at different ages. We found that the expression of NeuN was barely detected at P1 (Fig. S3B). At P5, NeuN expression became stronger in the deep sublayer, but not in the superficial sublayer of CA1 SP. At P7, the superficial sublayer started to have higher NeuN expression, and at P14, NeuN was abundantly expressed in both deep- and superficial-sublayers (Fig. S3B). This "first deep - then superficial" sequential NeuN expression indicates a sequence of birthtime-dependent neuronal maturation in CA1 SP. We also searched Allen Brain Atlas Developing Mouse Brain. Indeed, many marker proteins of glutamatergic synapses, including Shank3 (Fig. S3C), Homer-1, Camk2a, PSD-95, Synapsin-1 and Syntaxin 1 (Table S1), displayed a similar pattern: first expressed in the deep sublayer of SP at P4, then extended to the superficial sublayer and reached full expression at P14 (Fig. S3 and Table S1). This synapse maturation sequence aligns with the order of primary cilia protrusion from P5 to P14 first in the deep and then superficial sublayer of CA1 SP in both WT and Arl13b+ mice.

However, the case in the hippocampal CA3 region was different. Both WT and Arl13b+ had cilia expression at P5 and P7 almost at the same time in the deep and superficial sublayers of CA3 SP (Fig. S5). Likely, pyramidal neurons in the CA3 mature more simultaneously and several days earlier than CA1

neurons, as evidenced by NeuN expression pattern and strong expression of many glutamatergic synapse marker proteins including CamK2a in the CA3 at P4 (Fig. S5 and Table S1). This sharply contrasts with the weak and deep sublayer-restricted expression in the CA1 (Fig. S3 and Table S1). This data suggests that neuronal ciliation in the hippocampal CA1 region and neocortex concurs with neuronal maturation in an order of "first deep - then superficial", whereas the CA3 region does not display such a pattern in ciliation and maturation.

Late-born CA1 Principal Neurons Undergo a Reverse Movement to Adjust Their Position Postnatally.

We observed that cilia directionality changed from somewhat disorganized at P9 upon emanation to highly aligned at P14 (Fig. 1D), and cilia were initially clustered at the bottom of CA1 SP, then become more evenly distributed at P14 (Fig. 1D & 2C). We postulated that cilia/centrioles reversely move from SP bottom to the main SP. To test it, we examined centrioles/cilia distribution from P3 to P14 using Centrin2-GFP; Arl13b-mCherry mice, which mark centriole and primary cilia, respectively. The density of centriole in CA1 SP of these mice at P3-P7 was quite low (Fig. 3A), and a large fraction of centrioles was clustered at the SP bottom (Fig. 3A). However, a few days later at P10, cilia distribution became more even in SP (Fig. 3A), suggesting that the centrioles of late-born principal neurons migrate excessively to reach at SP bottom before reverse. We quantified nucleus density, centriole density, and the ratio of centriole to nucleus (C/N Ratio) in CA1 SP from P3 to P14 (Fig. 3B-E). First, Arl13b+ mice did not show significant differences in nucleus density at the middle and bottom panels from P3 to P14 in the dorsal CA1 SP (Fig. 3C). However, centrioles were highly condensed at SP bottom at P3 and P7 (Fig. 3D), and the C/N Ratio in SP bottom and SR were much higher than 1 (Fig. 3E). However, subsequently at P10 and P14, centrioles showed a relatively even distribution in the main SP (Fig. 3D). Consistently, C/N Ratio at P3 was about 2.5, but it decreased to around 1 at P14 (Fig. 3E).

Moreover, cilia density in the upper part of SP was very low at P7, while short primary cilia were highly condensed at SP bottom (Fig. 3F). At P10, neuronal primary cilia were elongated. Some centrioles/cilia became well-aligned with the radial axis, while others still clustered at SP bottom (Fig. 3F), suggesting that neurons move to the north, with centrioles taking the lead, followed by cilia tails. Afterwards at P14, cilia occupied the major space of SP, and their primary cilia almost uniformly pointed in the SR direction (not shown). A similar pattern was also observed in WT mice (Fig. 1D). We also quantified cilia orientation of the upper part of SP, which originally only had SO-pointing cilia at P7. Due to this "pull-back" cilia/centriole migration, more south-oriented cilia gradually moved up to the main SP from P7 to P14, the upper part of SP subsequently contained more south-oriented cilia (Fig. 3G-H). It is known that principal neurons migrate to the hippocampal and neocortical plates along radial glia fibers in a saltatory manner, in which the centrosome moves forward in the leading process, followed by nuclear translocation [23, 24, 52]. Here, the cilia/centrioles of late-born principal neurons in the superficial sublayer of CA1 SP move against the direction of radial migration to back to the main CA1 SP (Fig. 3I). We name this positioning process "reverse movement". Given SP lamina thickness reduced correspondingly (Fig. 1F), the change in centriole position also reflects the reverse movement of the cell body of principal neurons (Fig. 3I).

Principal Neurons in the Cerebral Cortex Move Backwards for Positioning and Lamina Refinement. The hippocampal CA1 region and neocortex share a birthtime-dependent inside-out lamination pattern [26, 53, 54]. To examine whether the neocortex has similarities to the CA1 SP in term of ciliation pattern and principal cell positioning, we examined ciliation timing, C/N Ratio, and cilia directionality in the postnatal mouse neocortex (Fig. 4). We found that primary cilia were not well protruded in the neocortical superficial sublayer until P7 (Fig. 4A-B). Like CA1 SP, neuronal primary cilia were expressed earlier in the deep sublayer than superficial sublayer in both WT and Arl13b+ mice (Fig. 4A-D). To determine if neocortical principal neurons are subjected to a reverse movement, we examined centriole/nuclei

distribution pattern in the outer layer of the neocortex at P3 and P14 (Fig. 4E-H). We manually drew top and middle panels on the outer layer to quantify centrioles and nuclei density (Fig. 4E). We found that the C/N ratios were near 1 and there were no significant differences between P3 and P14 and between the top and middle panels (Fig. 4F). However, the density of nuclei (Fig. 4G) and centrioles (Fig. 4H) at the top panel were higher than those at the middle panel at P3. But at P14, both centriole and nuclei density between two panels had no significant differences. This data indicates that the outer layer change from compact and uneven at P3 to sparse and even at P14, suggesting a reverse movement of somata. Consistently, the distances from the edge of the superficial sublayer to the pia gradually increase during the first two weeks after birth (Fig. 4I). Because primary cilia in the neocortex before P10 are too short to be accurately quantified for directionality (Fig. 4A-D), we thereby quantified cilia orientation in the neocortex using WT and Arl13b+ brain sections at P14 and P40, when primary cilia of principal neurons in the cerebral cortex exhibited a clear directionality. Primary cilia in both the superficial and deep sublayers of the neocortex orientated toward the pia in WT and Arl13b+ mice (Fig. 4J-K).

We next determined primary cilia directionality in other brain regions, including the subiculum, postsubiculum, cingulate cortex, entorhinal cortex, and piriform cortex. We found that projection neurons in compact laminae generally had opposite cilia directionality, while neurons in loosely layered laminae displayed a uniform cilia directionality (Fig. S6A-B, Table S2). We also compared cilia directionality in nucleated brain regions with laminated cortical regions. Primary cilia in the laminated cortical regions, such as the neocortex, hippocampal CA1, and subiculum, exhibited a clear directionality: they either had opposite cilia orientations or uniformly pointed in the direction of the pia (Fig. S6B). However, no clear primary cilia directionality was identified in many nucleated brain regions, including the thalamus, amygdala, and hypothalamus (Fig. S6A-B, Table S2). We further examined the cilia directionality of interneurons and astrocytes in the hippocampus and neocortex. Primary cilia of interneurons and astrocytes displayed irregular directionality (Fig. S6C-G, Table S2). This data demonstrates that principal neurons in laminated cortical regions display cilia directionality. We also observed that the clearest cilia

directionality manifests at P14 - P20 (Fig. 1-2 and Fig. S6), when principal neurons completed positioning. Together, these results suggest that it is the reverse movement of cell body of principal neurons during early postnatal neurodevelopment that leads to primary cilia directionality.

To confirm that principal cells in the neocortex indeed undergo a slow reverse movement during early postnatal development, we quantified the ratio of individual layer thickness relative to the whole six layers as well as the distance from Layer VI to the ventricular zone (VZ). We found that the thickness of superficial sublayer and deep sublayer changed drastically from E18.5 to P20. The superficial sublayer greatly expands, while the relative thickness of deep sublayer gradually decreased (Fig. S7A-D). In the meantime, the distance from the bottom of Layer VI to VZ significantly decreased with age postnatally (Fig. S7E-F). This data supports the conclusion that neocortical principal neurons have the space to move backwards during early postnatal development.

To further verify that neocortical principal neurons undergo a reverse movement during postnatal development, we developed a method that utilized CFSE dye to label cells in the outer layer (Layer II/III) of the neocortex at P0 and trace the location of labeled cells several days later. CFSE does not transfer to neighboring cells, allows for rapid labeling of cells within 30 minutes and sustains visibility for several weeks, providing an excellent tool to trace neuron migration *in vivo* [29, 55-57]. Firstly, CFSE dye stayed at the injection region, the outer layer of the superficial sublayer at P1, while at P3, many CFSE-labeled superficial neurons appeared in inner layers, and further inside of the neocortex at P9 (Fig. 5A-B). This data demonstrated that CFSE-labels cells undergo reverse movement and gradually move away from the outer layer. Because CFSE can label daughter cells[29, 58], EdU was also injected into E18.5 pregnant mice to label new-born cells after E18.5. Our results show that those CFSE-labeled migrating cells were not merged with EdU (Fig. 5B), excluding the possibility that the CFSE-positive cells were daughter cells of original labeled neurons. Secondly, to identify the cell type of reversely migrating cells, we used Ctip2 antibody, an early-born principal neuron marker, to stain CFSE-labeled brain sections. To our surprise, ~70% CFSE-labeled cells overlapped with Ctip2-marked cells (Fig. 5C-D), suggesting that CFSE-labeled

neurons were mostly excitatory neurons. To rule out the possibility that CFSE may diffuse into inner layers from the injection location, we also injected CFSE into inner cortical layers and found that CFSE injected into inner layers did not laterally spread to other regions (Fig. 5E). Together, these data confirm that principal neurons in the superficial sublayer of the neocortex exhibit a reverse movement during early postnatal development.

We also examined if subiculum and postsubiculum exhibit a similar reverse movement during early postnatal development by searching Allen Brain Atlas Developing Mouse Brain. We found that the demarcation between the distal CA1 and subiculum was not distinguishable at E18.5 and P4, but the compact CA1 - sparse subiculum distinction became prominent at P14 (Fig. S8, red arrows). This indicates that neurons in the subiculum, which are mostly Ctip2-positive neurons, undergo a more drastic reverse movement than CA1 principal neurons. Moreover, the curvature in the postsubiculum was not remarkable at P4 but became obvious at P14 due to reverse movement (Fig. S8, bule arrows). Together, based on our observation on reverse movement of centrioles (Fig. 1-3), CFSE cell tracing experiments (Fig. 5), postnatal changes in cortical lamination (Fig. S7-8), as well as *in situ* hybridization (ISH) data from Allen Brain Atlas, we estimated the speed of the reverse at different cerebral cortical regions (Table S3). While there are regional variations, the reverse speed was roughly 0.1-3 μm/hour, which is 10-30 fold slower than typical radial migration. Nevertheless, over time, the slow reverse movement can move a long distance and substantially re-shape laminar structure (Fig. S8).

Selective Disruption of Primary Cilia Function in the Forebrain Affects Brain Size, Principal Cell Positioning and Lamination.

Next, we asked if primary cilia regulate postnatal principal cell positioning. To selectively ablate or shorten primary cilia in the forebrain, we crossed Ift88 floxed strain [35] and Arl13b floxed strain [37] with Emx1-Cre mice, respectively, which expresses Cre selectively in the forebrain after E12.5 [59]. Immunostaining results indicated that primary cilia in Ift88 flox/flox Emx1-Cre conditional knockout

(Ift88 cKO) mice were deleted in the cerebral cortex but not in other brain regions or non-neuronal organs (not shown). Similarly, primary cilia were shortened selectively in the forebrain of Arl13b cKO mice using Emx1-Cre strain (not shown). We also included Arl13b+ mice for comparative phenotyping, which have elongated primary cilia, for a gain-of-function analysis (Fig. S2).

To globally investigate gross changes, we used X-ray micro-CT to scan the whole brains of P20 Ift88 cKO mice and littermate controls. Surprisingly, Ift88 cKO mice manifested gyrification in the granular retrosplenial cortex (RSG) (Fig. 6A), but not other regions throughout the brain. However, this regional gyrification was only observed in Ift88 cKO mice, not Arl13b cKO or Arl13b+ mice (not shown). Secondly, the neocortex thickness of Ift88 cKO mice was significantly higher than controls at P20 (Fig. 6A-B). We quantified the brain weights of Ift88 cKO mice from P0 to adulthood. Ift88 cKO mice did not show significant larger brain size in the embryonic stage (Fig. 6C), which is consistently with the published data [59]. But a larger brain started to appear at P5 and strong differences between Ift88 cKOs and WTs manifested at P5-P20 (Fig. 6C). Additionally, a low percentage of Ift88 cKO mice had spontaneous seizures after P14 (Fig. 6D). Together, Ift88 cKO mice exhibited cortical expansion, increased brain weight, and lower survival rate than controls. In contrast, Arl13b cKO mice only had slightly increased brain size at P9 but no significant difference at other ages (Fig. 6E). Conversely, the brain size of Arl13b+ mice before P9 was normal, but they had a smaller brain than controls after P14, when primary cilia were well expressed, and at P20 and P75 (Fig. 6F). These data suggest that primary cilia signaling modulate postnatal neurodevelopment.

We also examined neuronal composition in neocortical layers using Satb2 and Ctip2 antibodies, which are markers for late- and early-born principal neurons, respectively. Due to cortical expansion, the neocortical outer layer in Ift88 cKOs clearly had more neurons than controls (Fig. 6A). More interesting phenotype was in Layer V, which is typically occupied by Ctip2-positive neurons (Fig. 6G-I). There was no difference in Ctip2 neuronal number in Layer V between Ift88 cKO and controls from P0 to adulthood (Fig. 6H). Nevertheless, Layer V of Ift88 cKOs had more Satb2-positive neurons after P5, but not at P0 -

P3, than controls (Fig. 6I). Because radial migration of principal neurons is completed at P0 - P3, the difference in Layer V suggests that over-produced neurons in Ift88 KOs first migrate to the outer layer before P3 and then reversely move to the Layer V, thereby increasing the number of Sabt2-positive neurons in Layer V after P3. Consistently, ISH images from Allen Brain Atlas Developing Mouse Brain also show that Satb2-positive neurons are highly enriched in the outer layer at P1, less so at P3 and P7, while at P14 or after, Satb2 neurons become more evenly distributed among five neocortical layers. This evidence further supports the concept of reverse movement of principal neurons.

To understand how gyrification in Ift88 cKO mice is formed during postnatal development, we examined the developmental time-course of gyrification at different ages spanning from E18.5 to adulthood (Fig. 7A-C). We found that a shallow gyrus started to appear in RSG of Ift88 cKO at E18.5, and the degree of gyrification increased strongly from P0 to P9 and reached a steady state after P9 (Fig. 7A-C). Interestingly, the sulcus was formed via an invagination of the outer layer. This is probably because that too many principal neurons in the outer layer were squeezed in the confined RSG area and unable to expand forward. This consequently leads to invagination and forming a sulcus. We further discovered that not only the degree of gyrification, but also the distance from the midline to the edge of Layer II gradually increased with age (Fig. 7A-C), both of which are indicative of reverse movement. Additionally, we measured the distance from the midline to Layer V (marked by Ctip2) in RSG. Similarly, Layer V early-born neurons in RSG continuously moved backwards (Figure. 7D-E), as indicated by the increased distance from Layer V to the midline. These data provide additional evidence demonstrating that cortical principal neurons move backwards during postnatal development.

Next, we investigated the effects of cilia disruption on hippocampal neuron positioning. First, Ift88 cKO mice had abnormal CA1 SP compared to controls in the Satb2 and Ctip2 immunostaining (Fig. 8A-C). It is known that CA1 SP thickness gradually decreases with age (see Fig. S1A), partly due to cell apoptosis[60]. Ablation of primary cilia in Ift88 cKO mice caused delayed lamina condensation during P5-P9 (Fig. 8B-C), when primary cilia started to protrude primary cilia. Notably, the distal CA1 lamina

thickness of Ift88 cKO mice had been impacted more strongly than that of the proximal CA1 (Fig. 8A&D). Consistently, Arl13b cKO mice, which lost cilia directionality in the CA1 (Fig. 8D), also had misplaced CA1 principal neurons both in the deep and superficial sublayers (Fig. 8F). This data supports the notion that primary cilia regulate the positioning of hippocampal principal neurons.

To evaluate if primary cilia also modulate neuronal positioning in outside-in laminae, we examined cilia directionality and morphology in the granular cell layer of hippocampal dentate gyrus (DG). Primary cilia in DG are relatively short (Fig. S2), thus we leveraged Centrin2-GFP mice, which mark the base of primary cilia, to identify cilia orientation in DG. Neuronal primary cilia in the granule cell layer were oppositely orientated at P14 (Fig. 9A-B). Moreover, there was a developmental shift in Arl13b expression in primary cilia. Arl13b-labeled primary cilia were prominent at P9 but became much weaker at P20 (Fig. 9C), when AC3-labled primary cilia became more predominant (Fig. 9C). This expression pattern is reminiscent of the pattern in CA1 SP (Fig. 1A), supporting the role of primary cilia in cell positioning. We hypothesized that disruption of primary cilia function may affect neuronal positioning in the granule cell layer. Hence, we analyzed phenotypes in DG of Ift88 cKO and Arl13b cKO mice (Fig. 9D). We discovered that disruption of primary cilia function caused neuronal misplacement in the granular cell layer in DG in both Ift88 cKO and Arl13b cKO mice (Fig. 9E-G). The granular cell layer of both cKO mice lost compactness. There were many individual Ctip2-positive neurons sparsely distributed in the molecular layer. Of note, the degree of misplaced neurons in the molecular layer in Arl13b cKO mice was lower than in Ift88 cKO mice (Fig. 9G). Together, these data support the notion that primary cilia regulate the postnatal positioning of hippocampal principal neurons.

Discussion

This report presents robust evidence identifying reverse movement as a novel process for lamina refinement in the cerebral cortex: (1) Primary cilia of early- and late-born hippocampal neurons exhibit opposite orientations, whereas primary cilia of principal neurons in the neocortex, subiculum,

postsubiculum, entorhinal cortex and cingulate cortex generally point in the pia direction. (2) Principal neurons in the hippocampal CA1 superficial sublayer, subiculum, postsubiculum and neocortex undergo a slow reverse movement for postnatal cell positioning, which shapes laminae in the cerebral cortex. Primary cilia directionality serves as a "compass" that indicates the direction of the reverse movement and postnatal positioning of principal neurons in the cerebral cortex. (3) Selective ablation of primary cilia in the forebrain leads to cortical expansion, altered laminae, and cortical gyrification in the retrosplenial cortex, which manifest postnatally. The gyrification is formed via an invagination driven by cortical expansion and the reverse movement of principal cells. (4) Arl13b regulates the ciliation and postnatal positioning of hippocampal principal neurons.

The centriole/centrosome directs cellular microtubule dynamics that couple to nuclear translocation during radial migration [18, 23, 24, 57]. The centriole leads the radial migration of principal neuron during the embryonic development stage. It is not surprising that neuronal primary cilia do not fully arise until the completion of fast radial migration but protrude out during the positioning stage. After emanation, primary cilia indicate the positioning of early- and late-born principal neurons to the deep and superficial sublayers of CA1 SP (Fig. 1-3, S4). Ciliation timing and cilia directionality support that function: after principal neurons have migrated to the hippocampal plate, primary cilia first protrude out of early-born principal neurons and point north (Fig. 1-3), which is opposite to the direction of the radial migration. With delayed cilia protrusion, centrioles of late-born neurons migrate a longer distance, pass early-born neurons to reach the SP bottom and surprisingly congregate into a cluster. Afterwards, they start to express primary cilia and then reverse (Fig. 3). It is unclear yet whether the centrioles drive the reverse movement of the soma of principal neurons or simply primary cilia follow the reverse movement of cell bodies. Regardless, the movement of late-born neurons is opposite to the direction of radial migration (Fig. 3). The reverse movement finely adjusts the position of principal neurons. The role of primary cilia in regulating postnatal principal cell positioning is suggested by our genetic studies that conditionally manipulated primary cilia function. For example, selective ablation of primary cilia in the

forebrain in Ift88 cKO mice leads to altered lamination in the neocortex and hippocampal CA1 and DG (Fig. 6-9). Likewise, Arl13b cKO mice manifests similar phenotypes in the hippocampal CA1 and DG (Fig. 8-9).

It is known that excitatory synapses in the mouse hippocampal CA1 region are labile within the first two weeks after birth [47, 49, 61, 62]. However, it is unclear why CA1 principal neurons have to wait until p14 to form relatively stable synapses, and the electrophysiological features of synapses before P14 are different from those after P14 [47, 49, 61, 62]. We found that the centrioles of late-born neurons in CA1 SP undergo a marked reverse movement, over a distance of 10 - 35 μm, for postnatal positioning that completes around P14 (Fig. 1-3). This reverse movement may affect the cytoskeleton of dendrites and the stability of synapses. NeuN staining also revealed that late-born neurons in the hippocampus (Fig. S3B) and the neocortex (Fig. S3D) mature several days later than early-born neurons. These results align well with ISH data of numerous synaptic markers of Allen Brain Atlas. In contrast, primary cilia in the CA3 region does not clearly point towards specific directions. Neither centriole clustering in superficial sublayer nor marked reverse movement were identified in CA3 SP. Interestingly, CA3 principal neurons mature earlier and more simultaneously than CA1 neurons (Fig. S5). CA1 and neocortical principal neurons are subject to reverse movement for postnatal positioning during early postnatal development. Therefore, it is tempting to postulate that the delayed maturation of late-born neurons in the CA1 and the neocortex could be, at least in part, due to reverse movement or the delayed completion of cell positioning, while late-born and early-born CA3 principal neurons mature earlier and more simultaneously, likely due to lack of reverse movement.

Our analyses of cilia directionality led to the discovery of a slow backward movement of principle neurons during postnatal principal cell positioning. Primary cilia of principal neurons in the cerebral cortex spanning from the neocortex to the CA1 region display specific orientations. Primary cilia oriented oppositely in early- and late-born neurons in the compact CA1 SP as two groups of neurons move opposingly (Fig. 1-2). In contrast, neuronal primary cilia in the neocortical deep and superficial sublayers

exhibit a more uniformed orientation (Fig. 4, S4, S6), suggesting principal neurons reverse move toward the same direction. We have provided multiple lines of evidence showing that principal neurons in the neocortex are subject to a reverse movement for positioning during early postnatal development (Fig. 4-7, Fig. S7, Table S3), so do principal neurons in the subiculum and postsubiculum (Fig. S8). Primary cilia orientations in these areas indicate the direction of the reverse movement (Fig. S6). The mouse brain is composed of both laminated and non-laminated (or nucleated) structures. Laminated structures are typically found in the cerebral cortex. Non-laminated structures are found in other locations and do not possess distinct layers. While primary cilia of principal neurons exhibit a directionality in laminated brain regions, they have irregular orientations in non-laminar structures (Fig. S6). In addition, primary cilia of interneurons and astrocytes do not display specific directionality. All converges to support the notion that principal neurons in layered cortical regions display specific cilia directionality and it is the reverse movement of principal neurons that leads to specific cilia directionality.

One question arises why the cell body of principal neurons undergo a reverse movement for postnatal cell positioning. A short answer is if early-born neurons after arriving the hippocampal or neocortical plates did not move backwards to yield some space, late-arrived neurons would locate too close to these early-arrived neurons; then the inside-out lamination pattern was only able to form condensed layers, like the CA3 region in most mammalian species (Fig. S9). With a broader view, the mammalian cerebral cortex, particularly the human neocortex, can be likened to a "library" consisting of numerous shelves and layers of "books" (principal neurons). The development of such a sparsely layered, matrix-like architecture and its evolution from lower vertebrates to humans not only involves increased number of neurons and the needs of accommodating space, but also requires coordinated neuronal migration and positioning for placement. This permits orderly neuronal maturation and progressive circuit formation [33, 42, 63-65]. These processes are needed for the brain to acquire external information during postnatal development or learning processes to gradually construct well-organized neural circuitry to enable efficient information processing, storage, and retrieval. After the completion of radial migration,

the outer layer of neocortex is still highly condensed. Thus far, it is elusive why the mouse neocortical layers gradually become loosely layered, while the hippocampal CA1 and other allocortices become highly condensed. It is interesting that the CA1 SP in many species such as mice and ferrets is highly compact, that of macaques is markedly expanded and loosely layered [66], whereas those of roe deers, jackal and boar are somewhere in between (sparse in the deep sublayer but condensed in the superficial sub-layer) [67] (Fig. S9). Increased neurogenesis and postnatal neuronal apoptosis may contribute partly to changes in laminar cell density. However, if it were only apoptosis that caused sparse laminae, primary cilia of principal neurons could not always point in the pia direction. The cell density of five principal cell layers in the neocortex would be highly uneven, with very high density in Layer II/III and very low cell density in Layer I-IV. We propose that neuron radial migration stopped by Reelin before Layer I is not sufficient to construct sparsely layered inside-out laminae spanning from the neocortex to the subiculum in mice or to the CA1 in primates [66] (Fig. S9). An additional step of slow reverse movement is required for proper postnatal positioning and lamina refinement.

We propose a working model (Fig. S10), in which a slow reverse movement of principal neurons, coupled with fast radial migration and inside-out lamination pattern, is needed for fine-tuning lamination in the cerebral cortex (Table S3). (1) In compact lamina such as the mouse CA1 SP, late-born CA1 principal neurons reverse, whereas early-born neurons generally do not. Early- and late-born CA1 neurons continuously move against each other during postnatal development, gradually decreasing the lamina thickness (Fig. S1A and 3I). (2) In the subiculum, Ctip2-positive neurons move backwards significantly, encountering little impedance from other neurons. Consequently, subiculum develops into a sparse lamina distinct from the CA1 SP (Fig. S8). (3) In the neocortex and the neighboring entorhinal cortex and postsubiculum, both early- and late-born neurons undergo marked reverse movement postnatally (Fig. S7-8), gradually expanding the laminae and forming sparse five principal cell layers (Layer II-VI). Consistently, neuronal primary cilia of early- and late-born neurons orientate towards the pia direction (Fig. 4 and Fig. S6). (4) In some confined cortical regions, such as the RSG or cingulate cortex, over-

produced neurons in Ift88 cKO mice are forced to undergo a reverse movement to form a sulcus (Fig. 7). (5) We predict that loosely layered CA1 SP of primates (Fig. S9) is likely shaped by a remarkable reverse movement of principal neurons from the superficial sublayer (condensed region) toward the deep sublayer or the direction of the ventricular zone (sparse region). (6) In addition to affecting cortical layering, putatively the reverse movement may impact brain circuit development: the abundance of neurons in the outer layer of neocortex or the superficial sublayer of other cortical regions, such as the CA1 of mammals, could serve as a reservoir, from which neurons can gradually move reversely toward deep sublayer, become matured and form stable synaptic connectivity. This could influence the developmental order of neural circuitry. Together, the reverse movement of principal neurons for positioning can be potentially of great significance in both neurodevelopment and neurophysiology, which shape laminar configuration and modulate synaptic connectivity in the postnatal brain.

One may wonder why the reverse movement of principal neurons has not been reported previously. Possible reasons include: (1) It occurs postnatally after the radial migration has completed. Most studies on neuronal migration focus on the embryonic migration or postnatal neuronal migration in the rostral migrating stream. (2) The reverse movement is very slow, roughly 0.1-3 μm/hour, which is 10-30 fold slower than typical radial migration [68]. (3) Principal neurons generally reverse from a highly condensed layer to a sparser region (from the superficial to deep sublayer direction) (Fig. 1D, S7A, 7A). The high density of cells may prevent the observation of a slow backwards movement of individual neurons. (4) *Ex vivo* time-lapse imaging mostly used mice as a model, whose neocortex does not have gyrification. Gyrification formed by reverse movement might be easier to be detected if using primate or ferret neocortex. Ferret neocortical gyrification, which we interpret based on published MRI images of ferret brain development [69], is surprisingly formed by forward migration followed by a reverse movement during postnatal development. Further, although it is best known that the gyrification in the primate neocortex is driven by increased neurogenesis [70-72], the cellular mechanism of gyrification is not fully understood. We demonstrate that gyrification is, at least partly, driven by the reverse movement of

principal neurons. In summary, while further research is required, the new concept of reverse movement will open various research avenues to elucidate how principal neurons complete positioning in the cerebral cortex and how the sparse 6-layered neocortices evolved from the compact 3-layered allocortices.

Materials and Methods

Mice

All experiments are performed using mice with C57BL/6j genetic background. Ift88 floxed mice (Stock No. 022409), Arl13b floxed mice (Stock No. 031077), Emx1-Cre (Stock No. 005628) and Camk2a-Cre (T29-1) (Stock No. 005359) were purchased from the Jackson Laboratory (JAX). The Arl13b-mCherry Centrin2-GFP double transgenic mice (Stock No. 027967) were purchased from JAX and originally have C57Bl/6, BALB/c, and FVB/N mixed genetic background. The expression of Arl13b-mCherry and Centrin2-GFP are both driven by the pCAGGs promoter [41, 73, 74]. After importing to the Chen lab, we have backcrossed this strain with C57BL/6j mice for more than six generations to obtain uniform C57BL/6j background. The backcrossing has yielded three separate mouse lines: The backcrossing has also yielded three separate lines: one keeps as Arl13b-mCherry; Centrin2-GFP double transgenic mice (Arl13b+ mice), which will be used to mark primary cilia orientation. The other two are Arl13b-mCherry single and Centrin2-GFP single transgenic mice. Centrin2-GFP was used to mark centrioles which locate to the base of primary cilia. Mice were maintained on a 12-hour light/dark cycle at 22 °C and had access to food and water ad libitum. All animal procedures were approved by the Institutional Animal Care and Use Committee at the University of New Hampshire (UNH).

Brain Tissue Collection

Adult mice were deeply anesthetized with an intraperitoneal injection of ketamine and xylazine, and then were transcardially perfused with ice-cold 0.1 M phosphate buffer saline (PBS) followed by 4% paraformaldehyde (PFA) in 0.1 M PBS. Young pups (P0 - P7) were directly decapitated using a sharp

surgical scissors. Mouse brains were extracted and then placed into 4% PFA overnight at 4 °C. The following day, brains were rinsed in 0.1 M PBS for 30 min at room temperature. P0-P5 mouse brains then were dehydrated by 30% sucrose in 0.1 M PBS overnight at 4°C. Finally, those tissue were embedded in O.C.T resin before being sectioned at -18 °C using a cryostat to a thickness of 30 µm. P7 - P75 mouse brains were coronal sectioned using Compresstome (Precisionary Instruments LLC, NC) to a thickness of 30 - 50 µm.

Immunofluorescence Staining

E18.5-P5 mouse brains were sliced and mounted on gelatin-coated slices for immunostaining procedure, while P7 – P75 brain sections were sliced and placed in 24-wells plate, staying afloat during the staining procedure. They were washed three times with 0.1 M PBS. Then they were washed in 0.2% Triton X-100 (vol/vol) in 0.1 M PBS three times for 10 minutes at room temperature. Then they were blocked in blocking buffer (0.1M PBS containing 10% normal donkey serum (vol/vol), 2% bovine serum albumin (weight/vol), 0.2% Triton X-100 (vol/vol)) for one hour at room temperature. After that, slices were incubated with primary antibodies overnight at 4 °C in blocking buffer. After washing in 0.1 M PBS for three times for 10 minutes, slices were incubated with secondary antibodies for 2 hours at room temperature. Primary antibodies were rabbit anti-AC3 (1:10000, EnCor Biotechnology Inc., #RPCA-AC3), mouse anti-Arl13b (1:500, UC Davis clone N295B/66), mouse anti-calbindin (1:1000, Swant Switzerland, D-28K), rat anti-Ctip2 (1:500, Millipore-Sigma, MABE1045), rabbit anti-Satb2 (1:500, Abcam, ab92446), and mouse anti-NeuN (1:500, Millipore-Sigma, MAB377, clone A60). Secondary antibodies were Alexa Fluor 488-, 546-, or 647-conjugated (Invitrogen, La Jolla, CA). Finally, sections were counter-stained with DAPI (Southern Biotech, #OB010020) and images were acquired with confocal microscope (Nikon, A1R-HD), installed in the University Instrument Center at UNH.

Cilia Orientation Measurement

When a single primary cilium in WT mice was measured, the relatively thinner axoneme was defined as the tip and the opposite site as the base. For Arl13b-mCherry & Centrin2-GFP transgenic mice, the location of the primary cilium base was the same as Centrin2-GFP. The tails of most primary cilia in WT mice were straight and easy to determine their angles. However, primary cilia in the Arl13b-mCherry & Centrin2-GFP transgenic mice were much longer and showed kinks in their axoneme [41]. For those primary cilia, the initial part (~2 μm from the base) was used for determining the angle of those primary cilia. Fiji was utilized to measure the orientation of the single primary cilium. Four steps were used to complete a measurement. 1) First, the angle tool was selected among icons showed in the main window. 2) Then, the shift button on the keyboard was held, while left clicking the mouse meanwhile to draw a line (always from the right to left and parallel to the external capsule) to the location of the base of the primary cilium. 3) Afterwards, the shift button was released, and the mouse was left clicked to draw a line from the base to the tip of the primary cilium. 4) Lastly, while holding the control button and selecting "M" on the keyboard, the angle would jump out in a separate window. To measure the next primary cilium, steps 2-4 were repeated. Acquired data were finally exported as an excel file and then to a MATLAB program, which was used to generate polar plots.

Primary Cilia Length Measurement

We measured the length of primary cilia based on published methods [75], with modifications. The freehand line tool within Fiji (ImageJ) was used to measure cilia length from the base of axoneme to the distal tip.

CA1 SP Thickness Estimation

Confocal images of 20 μm Z-stack were used for quantifying CA1 SP thickness for both WT, Arl13b+ mice and Control mice. The straight-line tool within Fiji was used to measure CA1 SP thickness from the top of SP to the bottom of SP based on nucleus staining [76]. Because the nuclei at the top and bottom

edge of SP are not aligned to a straight line, this causes some variation of SP thickness. For young adult mice, we chose coronal sections at -1.9 mm posterior to Bregma to measure CA1 SP thickness. For young pups, we measured the thickness based on selected slices with hippocampal anatomic geometry similar to adult hippocampal sections. We acknowledge that our estimation method has limitations and stereotaxic accuracy needs to be improved. Nevertheless, it is known [76] that CA1 SP thickness decreases markedly with age, particularly during the first two weeks. We present CA1 SP thickness changes with ages to demonstrate that hippocampal principal cells maintain certain movement or re-positioning postnatally, yielding significant changes during early postnatal period (before P14) and mild adjustment afterwards.

Quantification of Nucleus Density, Centriole Density, and Centriole to Nucleus Ratio (C/N Ratio)

A 70 µm x 70 µm square box in SP was used for one single area quantification. The freehand line tool within Fiji was utilized to draw a line that matched the margin of the nucleus at the bottom of SP in the chosen box. This line was then vertically moved down 15 µm (to the SR direction) and up 15 µm (to the SO direction). The panel between two lines was defined as the bottom panel of SP for quantifying nucleus, centrioles, and C/N Ratio. The top line at the bottom panel of SP was further moved up 30 µm (to the SO direction). The area between the two lines (having a width of 30 µm) was defined as the middle panel of SP for the quantification of nuclei and centrioles. Since many centrioles were found to be clustered in the SR particularly in Arl13b+ mice, we also included a 15-µm-width area in the SR that was next to SP for quantification. Two Centrin2 dots were counted as one pair of centrioles, one DAPI separate round region were counted as one nucleus.

Normalized Brain Size/Weight

Due to the variation of maternal care and individual body sizes, the same batch of pups had variations in body weights and brain size. Thus, control littermates, cilia KO mice, or Arl13b+ mice differed by less than 10% in body weight were used to compare their brain size. To normalize brain size at different ages,

we first averaged the whole brain weights in controls from the same cage, then divided each mouse brain weight by this average number. Then a final normalized brain size for each mouse was completed.

Cortical Injection of CellTracer

CFDA-SE is carboxyfluorescein diacetate succinimidyl ester, whose acetyl group is responsible for the initial membrane permeability of the compound and is cleaved by intracellular esterases upon entry into the cell, giving rise to CFSE. CFSE is fluorescent and accumulates intracellularly and can maintain fluorescence for over one month. To label cells in the neocortex of neonatal pups, pups had 0.5 ul of 0.25 mM CFSE dye (Life Technologies, #C34572 and Dojindo Molecular Technologies, #C375) injected into the neocortex, covering the pial surface. The CFSE dye was colored with Fast Green to monitor successful injection. Pups were anesthetized by hypothermia by laying them on an ice bed (icebox filled with ice and cover it with aluminum foil. Anesthesia was assessed by the loss of movement. P0-1 pups would need 1–2 min to be anesthetized by laying it on top of the ice bed, P3 and P5 pups need 3–6 min on the ice bed[77]. The head of the anesthetized pup was placed in a head holder[78] and secured with a small piece of cloth tape. An injection needle or glass pipette which contained CFSE dye was inserted perpendicular to the cortical layer. CFSE dye was manually injected into the neocortex by slowly pushing the injection bottom on the pipette. If the injection was successful, the colored dye slowly spread under the skull, which were visible. The whole injection procedure were less than 8 minutes. Afterwards, pups were removed from the head holder and placed inside the recovery box on top of a heating mat for 10 minutes to achieve the normal body temperature, before gently returning the injected pups to their mother with the bedding.

EdU Injection and Staining

EdU (5-ethynyl-2-deoxyuridine, Carbosynth #: NE08701) was dissolved in saline at 1 mg/ml and stored at -20 °C. E18.5 pregnant mice were given one-time intraperitoneal injection of EdU (100 mg/kg). For staining EdU, fixed brain slices were permeabilized for 30 minutes in PBS + 0.2% Triton X-100, and

rinsed in PBS for 10 minutes, and then incubated in the fresh cocktail (Tris-buffered saline (100 mM final, pH 7.6), CuSO4 (4 mM final, Acros #197730010), Sulfo-Cyanine 3 Azide (2-5 uM final, Lumiprobe, #D1330), and fresh Sodium Ascorbate (100 mM final, freshly made each use, Acros, #352685000)) for 30-60 minutes. Lastly, rinsed brain slices 3 times in PBS for totally 30 minutes.

X-ray Micro-CT Scanning of Iodine-Stained Brains

Mice were anesthetized and transcardially perfused with ice-cold PBS, followed by ice-cold 4% PFA in PBS. Brain tissues were carefully dissected and post-fixed in 4% PFA in PBS for 3 days at 4ºC. Brains were dehydrated in ethanol grade series (30%, 50%, 70%, 80%, 90%) for 2 h followed by 7 days staining in 90% methanol plus 1% iodine solution at room temperature in a dark area (replace with fresh staining buffer every 2 days.). After staining, brains were rehydrated with 30% and 70% ethanol, for 1 hour each, at room temperature with mild agitation. Finally, brains samples were fixed in 1% agarose gel (Apex Bioresearch Products, #: 20-102GP) and placed in 5 ml tubes at 4ºC. All iodine-stained mouse brains were scanned using Zeiss 610 Versa X-Ray micro-CT scanner. The micro-CT scan was carried out in an air-conditioned cabinet at 80 kV acceleration voltage and 125 µA tube current, 0.16º rotation step through 360 degrees, giving rise to 2201 projections; no filter was used. Exposure time was 6 seconds, and 3 X-ray projections were acquired in each angle increment and averaged for reduction of noise. The achieved resolution was around 6 µm with isotropic voxels. Tomographic reconstruction was performed using Dragonfly 2020 software.

Quantification of Misplaced Ctip2-stained Neurons in DG

We quantified misplaced Ctip2-neurons in the molecular layer of DG as indicated in Fig. 9F. Fiji was utilized to count the cell numbers. Firstly, the freehand line was selected among icons showed in the main window, then drawing a line which almost adjoined and covered the full outmost edge of granule cell layer (GCL) in the top layer and selecting “M” on the keyboard. Next, drawing several lines which is 20

μm, 30 μm, 50 μm perpendicular to the first line. Then copying the first line and move it parallelly to the end point of those 20 μm, 30 μm, 50 μm lines. After finishing this area selection step, the Plugins > Analyze > Cell Counter was selected among icons showed in the main window, after cell counter window showed up, first initializing the image, and then counting.

Statistical and Software

Data were analyzed with Fiji, GraphPad Prism and MATLAB. Data was considered as statistically significant if $p < 0.05$ and values in the graph are expressed as mean ± standard error of the mean (SEM). Statistical analyses were conducted using ANOVA for multiple group comparison or Student's T-test with a two-tailed distribution, as appropriate. If not otherwise indicated in the text or Fig. legends, N.S., Not Significant; * $p < 0.05$; ** $p < 0.01$; *** $p < 0.001$.

References:

1. Bishop GA, Berbari NF, Lewis J, Mykytyn K. Type III adenylyl cyclase localizes to primary cilia throughout the adult mouse brain. J Comp Neurol. 2007;505(5):562-71. doi: 10.1002/cne.21510. PubMed PMID: 17924533.
2. Sterpka A, Chen X. Neuronal and astrocytic primary cilia in the mature brain. Pharmacol Res. 2018;137:114-21. doi: 10.1016/j.phrs.2018.10.002. PubMed PMID: 30291873; PubMed Central PMCID: PMC6410375.
3. Singla V, Reiter JF. The primary cilium as the cell's antenna: signaling at a sensory organelle. Science. 2006;313(5787):629-33. doi: 10.1126/science.1124534. PubMed PMID: 16888132.
4. Valente EM, Rosti RO, Gibbs E, Gleeson JG. Primary cilia in neurodevelopmental disorders. Nat Rev Neurol. 2014;10(1):27-36. doi: 10.1038/nrneurol.2013.247. PubMed PMID: 24296655; PubMed Central PMCID: PMC3989897.
5. Lee JE, Gleeson JG. Cilia in the nervous system: linking cilia function and neurodevelopmental disorders. Curr Opin Neurol. 2011;24(2):98-105. doi: 10.1097/WCO.0b013e3283444d05. PubMed PMID: 21386674; PubMed Central PMCID: PMC3984876.
6. Guemez-Gamboa A, Coufal NG, Gleeson JG. Primary cilia in the developing and mature brain. Neuron. 2014;82(3):511-21. doi: 10.1016/j.neuron.2014.04.024. PubMed PMID: 24811376; PubMed Central PMCID: PMC4104280.
7. Lee JH, Gleeson JG. The role of primary cilia in neuronal function. Neurobiol Dis. 2010;38(2):167-72. doi: 10.1016/j.nbd.2009.12.022. PubMed PMID: 20097287; PubMed Central PMCID: PMC2953617.
8. Park SM, Jang HJ, Lee JH. Roles of Primary Cilia in the Developing Brain. Front Cell Neurosci. 2019;13:218. doi: 10.3389/fncel.2019.00218. PubMed PMID: 31139054; PubMed Central PMCID: PMC6527876.

9. Hasenpusch-Theil K, Theil T. The Multifaceted Roles of Primary Cilia in the Development of the Cerebral Cortex. Front Cell Dev Biol. 2021;9:630161. doi: 10.3389/fcell.2021.630161. PubMed PMID: 33604340; PubMed Central PMCID: PMCPMC7884624.
10. Pal K, Mukhopadhyay S. Primary cilium and sonic hedgehog signaling during neural tube patterning: role of GPCRs and second messengers. Dev Neurobiol. 2015;75(4):337-48. doi: 10.1002/dneu.22193. PubMed PMID: 24863049.
11. Mukhopadhyay S, Wen X, Ratti N, Loktev A, Rangell L, Scales SJ, et al. The ciliary G-protein-coupled receptor Gpr161 negatively regulates the Sonic hedgehog pathway via cAMP signaling. Cell. 2013;152(1-2):210-23. doi: 10.1016/j.cell.2012.12.026. PubMed PMID: 23332756.
12. Dessaud E, McMahon AP, Briscoe J. Pattern formation in the vertebrate neural tube: a sonic hedgehog morphogen-regulated transcriptional network. Development. 2008;135(15):2489-503. doi: 10.1242/dev.009324. PubMed PMID: 18621990.
13. Gorivodsky M, Mukhopadhyay M, Wilsch-Braeuninger M, Phillips M, Teufel A, Kim C, et al. Intraflagellar transport protein 172 is essential for primary cilia formation and plays a vital role in patterning the mammalian brain. Dev Biol. 2009;325(1):24-32. doi: 10.1016/j.ydbio.2008.09.019. PubMed PMID: 18930042; PubMed Central PMCID: PMCPMC2613858.
14. Higginbotham H, Guo J, Yokota Y, Umberger NL, Su CY, Li J, et al. Arl13b-regulated cilia activities are essential for polarized radial glial scaffold formation. Nat Neurosci. 2013;16(8):1000-7. doi: 10.1038/nn.3451. PubMed PMID: 23817546; PubMed Central PMCID: PMCPMC3866024.
15. Sheu SH, Upadhyayula S, Dupuy V, Pang S, Deng F, Wan J, et al. A serotonergic axon-cilium synapse drives nuclear signaling to alter chromatin accessibility. Cell. 2022;185(18):3390-407 e18. doi: 10.1016/j.cell.2022.07.026. PubMed PMID: 36055200; PubMed Central PMCID: PMCPMC9789380.
16. Amador-Arjona A, Elliott J, Miller A, Ginbey A, Pazour GJ, Enikolopov G, et al. Primary cilia regulate proliferation of amplifying progenitors in adult hippocampus: implications for learning and memory. J Neurosci. 2011;31(27):9933-44. doi: 10.1523/JNEUROSCI.1062-11.2011. PubMed PMID: 21734285; PubMed Central PMCID: PMCPMC3758574.
17. Breunig JJ, Sarkisian MR, Arellano JI, Morozov YM, Ayoub AE, Sojitra S, et al. Primary cilia regulate hippocampal neurogenesis by mediating sonic hedgehog signaling. Proc Natl Acad Sci U S A. 2008;105(35):13127-32. doi: 10.1073/pnas.0804558105. PubMed PMID: 18728187; PubMed Central PMCID: PMCPMC2529104.
18. Marin O, Valiente M, Ge X, Tsai LH. Guiding neuronal cell migrations. Cold Spring Harb Perspect Biol. 2010;2(2):a001834. doi: 10.1101/cshperspect.a001834. PubMed PMID: 20182622; PubMed Central PMCID: PMCPMC2828271.
19. Marin O, Rubenstein JL. Cell migration in the forebrain. Annu Rev Neurosci. 2003;26:441-83. doi: 10.1146/annurev.neuro.26.041002.131058. PubMed PMID: 12626695.
20. Hatten ME. Central nervous system neuronal migration. Annu Rev Neurosci. 1999;22:511-39. doi: 10.1146/annurev.neuro.22.1.511. PubMed PMID: 10202547.
21. Tsai LH, Gleeson JG. Nucleokinesis in neuronal migration. Neuron. 2005;46(3):383-8. doi: 10.1016/j.neuron.2005.04.013. PubMed PMID: 15882636.
22. Rahimi-Balaei M, Bergen H, Kong J, Marzban H. Neuronal Migration During Development of the Cerebellum. Front Cell Neurosci. 2018;12:484. doi: 10.3389/fncel.2018.00484. PubMed PMID: 30618631; PubMed Central PMCID: PMCPMC6304365.
23. Kuijpers M, Hoogenraad CC. Centrosomes, microtubules and neuronal development. Mol Cell Neurosci. 2011;48(4):349-58. doi: 10.1016/j.mcn.2011.05.004. PubMed PMID: 21722732.
24. Higginbotham HR, Gleeson JG. The centrosome in neuronal development. Trends Neurosci. 2007;30(6):276-83. doi: 10.1016/j.tins.2007.04.001. PubMed PMID: 17420058.
25. Cembrowski MS, Spruston N. Heterogeneity within classical cell types is the rule: lessons from hippocampal pyramidal neurons. Nat Rev Neurosci. 2019;20(4):193-204. doi: 10.1038/s41583-019-0125-5. PubMed PMID: 30778192.

26. Soltesz I, Losonczy A. CA1 pyramidal cell diversity enabling parallel information processing in the hippocampus. Nat Neurosci. 2018;21(4):484-93. doi: 10.1038/s41593-018-0118-0. PubMed PMID: 29593317; PubMed Central PMCID: PMCPMC5909691.
27. Khalaf-Nazzal R, Francis F. Hippocampal development - old and new findings. Neuroscience. 2013;248:225-42. doi: 10.1016/j.neuroscience.2013.05.061. PubMed PMID: 23756184.
28. Kriegstein AR, Noctor SC. Patterns of neuronal migration in the embryonic cortex. Trends Neurosci. 2004;27(7):392-9. doi: 10.1016/j.tins.2004.05.001. PubMed PMID: 15219738.
29. Yoshinaga S, Shin M, Kitazawa A, Ishii K, Tanuma M, Kasai A, et al. Comprehensive characterization of migration profiles of murine cerebral cortical neurons during development using FlashTag labeling. iScience. 2021;24(4):102277. doi: 10.1016/j.isci.2021.102277. PubMed PMID: 33851097; PubMed Central PMCID: PMCPMC8022222.
30. Moffat JJ, Ka M, Jung EM, Kim WY. Genes and brain malformations associated with abnormal neuron positioning. Mol Brain. 2015;8(1):72. doi: 10.1186/s13041-015-0164-4. PubMed PMID: 26541977; PubMed Central PMCID: PMCPMC4635534.
31. Liu X, Zheng J, Qi S, Shen Q. NONO Regulates Cortical Neuronal Migration and Postnatal Neuronal Maturation. Neurosci Bull. 2019;35(6):1097-101. doi: 10.1007/s12264-019-00428-y. PubMed PMID: 31502212; PubMed Central PMCID: PMCPMC6864022.
32. Yang J, Qiu L, Chen X. Neuronal primary cilia regulate pyramidal cell positioning to the deep and superficial sublayers in the hippocampal CA1. BioRxiv. 2021. doi: 10.1101/2021.12.21.473383.
33. Geschwind DH, Rakic P. Cortical evolution: judge the brain by its cover. Neuron. 2013;80(3):633-47. doi: 10.1016/j.neuron.2013.10.045. PubMed PMID: 24183016; PubMed Central PMCID: PMCPMC3922239.
34. Gorski JA, Talley T, Qiu M, Puelles L, Rubenstein JL, Jones KR. Cortical excitatory neurons and glia, but not GABAergic neurons, are produced in the Emx1-expressing lineage. J Neurosci. 2002;22(15):6309-14. doi: 20026564. PubMed PMID: 12151506.
35. Haycraft CJ, Zhang Q, Song B, Jackson WS, Detloff PJ, Serra R, et al. Intraflagellar transport is essential for endochondral bone formation. Development. 2007;134(2):307-16. doi: 10.1242/dev.02732. PubMed PMID: 17166921.
36. Berbari NF, Malarkey EB, Yazdi SM, McNair AD, Kippe JM, Croyle MJ, et al. Hippocampal and cortical primary cilia are required for aversive memory in mice. PLoS One. 2014;9(9):e106576. doi: 10.1371/journal.pone.0106576. PubMed PMID: 25184295; PubMed Central PMCID: PMC4153651.
37. Su CY, Bay SN, Mariani LE, Hillman MJ, Caspary T. Temporal deletion of Arl13b reveals that a mispatterned neural tube corrects cell fate over time. Development. 2012;139(21):4062-71. doi: 10.1242/dev.082321. PubMed PMID: 23014696; PubMed Central PMCID: PMCPMC3472586.
38. Chen X, Luo J, Leng Y, Yang Y, Zweifel LS, Palmiter RD, et al. Ablation of Type III Adenylyl Cyclase in Mice Causes Reduced Neuronal Activity, Altered Sleep Pattern, and Depression-like Phenotypes. Biol Psychiatry. 2016;80(11):836-48. doi: 10.1016/j.biopsych.2015.12.012. PubMed PMID: 26868444.
39. Yang J, Qiu L, Strobel M, Kabel A, Zha XM, Chen X. Acid-Sensing Ion Channels Contribute to Type III Adenylyl Cyclase-Independent Acid Sensing of Mouse Olfactory Sensory Neurons. Mol Neurobiol. 2020. doi: 10.1007/s12035-020-01943-0. PubMed PMID: 32458389.
40. Zhou Y, Qiu L, Sterpka A, Wang H, Chu F, Chen X. Comparative Phosphoproteomic Profiling of Type III Adenylyl Cyclase Knockout and Control, Male, and Female Mice. Front Cell Neurosci. 2019;13:34. doi: 10.3389/fncel.2019.00034. PubMed PMID: 30814930; PubMed Central PMCID: PMC6381875.
41. Sterpka A, Yang J, Strobel M, Zhou Y, Pauplis C, Chen X. Diverged morphology changes of astrocytic and neuronal primary cilia under reactive insults. Mol Brain. 2020;13(1):28. doi: 10.1186/s13041-020-00571-y. PubMed PMID: 32122360; PubMed Central PMCID: PMC7053156.

42. Wong FK, Marin O. Developmental Cell Death in the Cerebral Cortex. Annu Rev Cell Dev Biol. 2019;35:523-42. doi: 10.1146/annurev-cellbio-100818-125204. PubMed PMID: 31283379.
43. Valero M, Cid E, Averkin RG, Aguilar J, Sanchez-Aguilera A, Viney TJ, et al. Determinants of different deep and superficial CA1 pyramidal cell dynamics during sharp-wave ripples. Nat Neurosci. 2015;18(9):1281-90. doi: 10.1038/nn.4074. PubMed PMID: 26214372; PubMed Central PMCID: PMCPMC4820637.
44. Larkins CE, Aviles GD, East MP, Kahn RA, Caspary T. Arl13b regulates ciliogenesis and the dynamic localization of Shh signaling proteins. Mol Biol Cell. 2011;22(23):4694-703. doi: 10.1091/mbc.E10-12-0994. PubMed PMID: 21976698; PubMed Central PMCID: PMC3226485.
45. Gigante ED, Taylor MR, Ivanova AA, Kahn RA, Caspary T. ARL13B regulates Sonic hedgehog signaling from outside primary cilia. Elife. 2020;9. doi: 10.7554/eLife.50434. PubMed PMID: 32129762; PubMed Central PMCID: PMCPMC7075693.
46. Radic T, Friess L, Vijikumar A, Jungenitz T, Deller T, Schwarzacher SW. Differential Postnatal Expression of Neuronal Maturation Markers in the Dentate Gyrus of Mice and Rats. Front Neuroanat. 2017;11:104. doi: 10.3389/fnana.2017.00104. PubMed PMID: 29184486; PubMed Central PMCID: PMCPMC5694555.
47. Fiala JC, Feinberg M, Popov V, Harris KM. Synaptogenesis via dendritic filopodia in developing hippocampal area CA1. J Neurosci. 1998;18(21):8900-11. doi: 10.1523/JNEUROSCI.18-21-08900.1998. PubMed PMID: 9786995; PubMed Central PMCID: PMCPMC6793554.
48. Lauri SE, Vesikansa A, Segerstrale M, Collingridge GL, Isaac JT, Taira T. Functional maturation of CA1 synapses involves activity-dependent loss of tonic kainate receptor-mediated inhibition of glutamate release. Neuron. 2006;50(3):415-29. doi: 10.1016/j.neuron.2006.03.020. PubMed PMID: 16675396.
49. Thakar S, Wang L, Yu T, Ye M, Onishi K, Scott J, et al. Evidence for opposing roles of Celsr3 and Vangl2 in glutamatergic synapse formation. Proceedings of the National Academy of Sciences of the United States of America. 2017;114(4):E610-E8. doi: 10.1073/pnas.1612062114. PubMed PMID: 28057866; PubMed Central PMCID: PMC5278468.
50. Sarnat HB, Nochlin D, Born DE. Neuronal nuclear antigen (NeuN): a marker of neuronal maturation in early human fetal nervous system. Brain Dev. 1998;20(2):88-94. doi: 10.1016/s0387-7604(97)00111-3. PubMed PMID: 9545178.
51. Gusel'nikova VV, Korzhevskiy DE. NeuN As a Neuronal Nuclear Antigen and Neuron Differentiation Marker. Acta Naturae. 2015;7(2):42-7. PubMed PMID: 26085943; PubMed Central PMCID: PMCPMC4463411.
52. Rahimi-Balaei M, Bergen H, Kong J, Marzban H. Neuronal Migration During Development of the Cerebellum. Frontiers in Cellular Neuroscience. 2018;12(484). doi: 10.3389/fncel.2018.00484.
53. Cooper JA. A mechanism for inside-out lamination in the neocortex. Trends Neurosci. 2008;31(3):113-9. doi: 10.1016/j.tins.2007.12.003. PubMed PMID: 18255163.
54. Forster E, Zhao S, Frotscher M. Laminating the hippocampus. Nat Rev Neurosci. 2006;7(4):259-67. doi: 10.1038/nrn1882. PubMed PMID: 16543914.
55. Telley L, Govindan S, Prados J, Stevant I, Nef S, Dermitzakis E, et al. Sequential transcriptional waves direct the differentiation of newborn neurons in the mouse neocortex. Science. 2016;351(6280):1443-6. doi: 10.1126/science.aad8361. PubMed PMID: 26940868.
56. Govindan S, Oberst P, Jabaudon D. In vivo pulse labeling of isochronic cohorts of cells in the central nervous system using FlashTag. Nat Protoc. 2018;13(10):2297-311. doi: 10.1038/s41596-018-0038-1. PubMed PMID: 30258174.
57. Stoufflet J, Chaulet M, Doulazmi M, Fouquet C, Dubacq C, Metin C, et al. Primary cilium-dependent cAMP/PKA signaling at the centrosome regulates neuronal migration. Sci Adv. 2020;6(36). doi: 10.1126/sciadv.aba3992. PubMed PMID: 32917588; PubMed Central PMCID: PMCPMC7467704.

58. Telley L, Govindan S, Prados J, Stevant I, Nef S, Dermitzakis E, et al. Sequential transcriptional waves direct the differentiation of newborn neurons in the mouse neocortex. Science (New York, NY). 2016;351(6280):1443-6. doi: doi:10.1126/science.aad8361.
59. Snedeker J, Schock EN, Struve JN, Chang C-F, Cionni M, Tran PV, et al. Unique spatiotemporal requirements for intraflagellar transport genes during forebrain development. PloS one. 2017;12(3):e0173258. doi: 10.1371/journal.pone.0173258.
60. Pönniö T, Conneely OM. nor-1 regulates hippocampal axon guidance, pyramidal cell survival, and seizure susceptibility. Molecular and cellular biology. 2004;24(20):9070-8. Epub 2004/10/01. doi: 10.1128/mcb.24.20.9070-9078.2004. PubMed PMID: 15456880; PubMed Central PMCID: PMCPmc517886.
61. Hsia AY, Malenka RC, Nicoll RA. Development of excitatory circuitry in the hippocampus. Journal of neurophysiology. 1998;79(4):2013-24. doi: 10.1152/jn.1998.79.4.2013. PubMed PMID: 9535965.
62. Lauri SE, Segerstrale M, Vesikansa A, Maingret F, Mulle C, Collingridge GL, et al. Endogenous activation of kainate receptors regulates glutamate release and network activity in the developing hippocampus. The Journal of neuroscience : the official journal of the Society for Neuroscience. 2005;25(18):4473-84. doi: 10.1523/JNEUROSCI.4050-04.2005. PubMed PMID: 15872094; PubMed Central PMCID: PMC6725041.
63. Franchini LF. Genetic Mechanisms Underlying Cortical Evolution in Mammals. Front Cell Dev Biol. 2021;9:591017. doi: 10.3389/fcell.2021.591017. PubMed PMID: 33659245; PubMed Central PMCID: PMCPMC7917222.
64. Karten HJ. Vertebrate brains and evolutionary connectomics: on the origins of the mammalian 'neocortex'. Philos Trans R Soc Lond B Biol Sci. 2015;370(1684). doi: 10.1098/rstb.2015.0060. PubMed PMID: 26554047; PubMed Central PMCID: PMCPMC4650131.
65. Karten HJ, Shimizu T. The origins of neocortex: connections and lamination as distinct events in evolution. J Cogn Neurosci. 1989;1(4):291-301. doi: 10.1162/jocn.1989.1.4.291. PubMed PMID: 23971981.
66. Bachevalier J. Nonhuman primate models of hippocampal development and dysfunction. Proc Natl Acad Sci U S A. 2019;116(52):26210-6. doi: 10.1073/pnas.1902278116. PubMed PMID: 31871159; PubMed Central PMCID: PMCPMC6936345.
67. Malikovic J, Amrein I, Vinciguerra L, Lalosevic D, Wolfer DP, Slomianka L. Cell numbers in the reflected blade of CA3 and their relation to other hippocampal principal cell populations across seven species. Front Neuroanat. 2022;16:1070035. doi: 10.3389/fnana.2022.1070035. PubMed PMID: 36686574; PubMed Central PMCID: PMCPMC9846821.
68. Tabata H, Nakajima K. Multipolar Migration: The Third Mode of Radial Neuronal Migration in the Developing Cerebral Cortex. The Journal of Neuroscience. 2003;23(31):9996-10001. doi: 10.1523/jneurosci.23-31-09996.2003.
69. Barnette AR, Neil JJ, Kroenke CD, Griffith JL, Epstein AA, Bayly PV, et al. Characterization of brain development in the ferret via MRI. Pediatr Res. 2009;66(1):80-4. doi: 10.1203/PDR.0b013e3181a291d9. PubMed PMID: 19287340; PubMed Central PMCID: PMCPMC3384539.
70. Ronan L, Voets N, Rua C, Alexander-Bloch A, Hough M, Mackay C, et al. Differential tangential expansion as a mechanism for cortical gyrification. Cereb Cortex. 2014;24(8):2219-28. doi: 10.1093/cercor/bht082. PubMed PMID: 23542881; PubMed Central PMCID: PMCPMC4089386.
71. Ronan L, Fletcher PC. From genes to folds: a review of cortical gyrification theory. Brain Struct Funct. 2015;220(5):2475-83. doi: 10.1007/s00429-014-0961-z. PubMed PMID: 25511709; PubMed Central PMCID: PMCPMC4549381.
72. Fernandez V, Borrell V. Developmental mechanisms of gyrification. Curr Opin Neurobiol. 2023;80:102711. doi: 10.1016/j.conb.2023.102711. PubMed PMID: 37001342.

73. Bangs FK, Schrode N, Hadjantonakis AK, Anderson KV. Lineage specificity of primary cilia in the mouse embryo. Nat Cell Biol. 2015;17(2):113-22. doi: 10.1038/ncb3091. PubMed PMID: 25599390; PubMed Central PMCID: PMC4406239.
74. Higginbotham H, Bielas S, Tanaka T, Gleeson JG. Transgenic mouse line with green-fluorescent protein-labeled Centrin 2 allows visualization of the centrosome in living cells. Transgenic Res. 2004;13(2):155-64. doi: 10.1023/b:trag.0000026071.41735.8e. PubMed PMID: 15198203.
75. Sipos E, Komoly S, Acs P. Quantitative Comparison of Primary Cilia Marker Expression and Length in the Mouse Brain. J Mol Neurosci. 2018;64(3):397-409. doi: 10.1007/s12031-018-1036-z. PubMed PMID: 29464516.
76. Ponnio T, Conneely OM. nor-1 regulates hippocampal axon guidance, pyramidal cell survival, and seizure susceptibility. Mol Cell Biol. 2004;24(20):9070-8. doi: 10.1128/MCB.24.20.9070-9078.2004. PubMed PMID: 15456880; PubMed Central PMCID: PMCPMC517886.
77. Oomoto I, Uwamori H, Matsubara C, Odagawa M, Kobayashi M, Kobayashi K, et al. Protocol for cortical-wide field-of-view two-photon imaging with quick neonatal adeno-associated virus injection. STAR protocols. 2021;2(4):101007. Epub 2021/12/25. doi: 10.1016/j.xpro.2021.101007. PubMed PMID: 34950887; PubMed Central PMCID: PMCPmc8672102.
78. Olivetti PR, Lacefield CO, Kellendonk C. A device for stereotaxic viral delivery into the brains of neonatal mice. 2020;69(4):307-12. doi: 10.2144/btn-2020-0050. PubMed PMID: 32777950.
79. Oshima K, Yoshinaga S, Kitazawa A, Hirota Y, Nakajima K, Kubo K-i. A Unique "Reversed" Migration of Neurons in the Developing Claustrum. The Journal of Neuroscience. 2023;43:693 - 708.
80. Borrell V, Kaspar BK, Gage FH, Callaway EM. In vivo Evidence for Radial Migration of Neurons by Long-Distance Somal Translocation in the Developing Ferret Visual Cortex. Cerebral Cortex. 2005;16(11):1571-83. doi: 10.1093/cercor/bhj094.

Figure Legends:

Fig. 1. Opposite primary cilia orientation in the deep and superficial sublayers of CA1 SP. (A) Primary cilia morphology and orientation were subject to marked change with ages from P5 to ~P75. Scale bars: 10 µm. **(B)** A diagram showing cilia orientation measurement in the dorsal hippocampal CA1 SP. Cilia shown in the SP are posited in the polar plot on the bottom. Polar plot analyses were performed to determine primary cilia orientation distribution. The numbers (0-360º) on the out circles denote the degree of cilia orientation relative to the external capsule, and the numbers on concentric circles are the percentage of cilia orientation at specific angles. **(C)** Most primary cilia pointed in the SR direction (180º - 360º) in polar plots (Left). The histogram plots (binned in 10-degree intervals) present the percentage of cilia at different angles. The degrees in polar plots were converted to histogram plots by subtracting 180º. **(D)** Primary cilia abundantly emerged in the SP bottom at ~P9, and their distribution and directionality drastically changed from P9 to P14. Cyan arrows indicate the direction of cilia distribution (from the

bottom to the top). Scale bars: 20 µm. **(E)** The percentage of north-oriented cilia decreased significantly from P10 to P40. **(F)** The thickness of SP lamina in the hippocampal CA1 decreased significantly from P3 - P75. Each triangle in **E-F** represents one location in SP for quantification. One-way ANOVA with Bonferroni's multiple comparison test. **(G)** Primary cilia of calbindin-positive neurons at P40 mostly orientated toward the SR direction, while calbindin-negative neurons' cilia generally pointed in the SO direction. The white boxes are enlarged at the bottom. Super: superficial sublayer; Deep, deep sublayer. SP: stratum pyramidale; SO: stratum oriens; SR: stratum radiatum.

Fig. 2. Opposite primary cilia orientation in the hippocampal SP of Arl13b+ mice. (A) Early-born neurons in the deep sublayer protruded cilia earlier than neurons in the superficial sublayers at P3 for both WT mice and Arl13b+ mice, and those early-protruding cilia pointed north. **(A-B)** At P7, WT (left) had few cilia in SP. Nevertheless, at P10 cilia were abundantly expressed. Transgenic expression of Arl13b in Arl13b+ mice (right) elongated cilia length and promoted earlier cilia expression. Cilia in the deep sublayer orientated towards SO, whereas cilia in superficial sublayer pointed in the SR direction. **(C)** Primary cilia orientation changes at P7, P10, and P14. White boxes were enlarged at the bottom. White arrows indicate the mother centriole or the base of cilium, green arrows denote some Centrin2-GFP artifacts. Scale bars: 10 µm top, zoom in 5 µm at the bottom. **(D)** Polar plots and histogram plots of cilia orientation of Arl13b+ mice from P7-P75. **(E)** The percentage of north-oriented cilia at different ages of Arl13b+ mice. One-way ANOVA with Bonferroni's multiple comparison test. **(F)** The percentage of north-oriented cilia in WT compared to ARl13b+ mice. Each triangle represents the percentage of north-oriented cilia from an area of CA1 SP for quantifying cilia orientation (**E-F**). **(G)** Primary cilia of calbindin-positive neurons (purple) at P40 Arl13b+ mice mostly pointed in the SR direction, while calbindin-negative neurons' cilia generally pointed in the SO direction. The white boxes are enlarged at the bottom.

Fig. 3. Centriole/cilia of late-born neurons are clustered at hippocampal SP bottom before a reverse movement. (A) Arl13b+ mice displayed a clustering pattern of centrioles in SP bottom before P7, and then re-distributed back to the main SP afterwards. Scale bars: 10 µm. **(B)** For centriole quantification, we manually separated the SP into top, middle, and bottom panels and included a panel of SR (15 µm) because some centrioles further reached SR. An example is shown using P3 SP. Scale bars: 10 µm. **(C-D)** Quantification of the number of nuclei and centrioles per square millimeter (nuclei/mm^2 and centriole/mm^2) in the middle and bottom panels of SP from P3 to P14. B: bottom; M: middle. Two-way ANOVA with Bonferroni's multiple comparison test. **(E)** Centriole/Nucleus ratio at SP bottom and SR from P3 to P14. **(F)** Enlarged cilia images of late-born neurons showing that cilia length was increasing, and cilia and centrioles were migrating upward (indicated by cyan arrows) at P7 and P10. Centrioles (white arrows) in the front were followed by cilia axoneme. Scale bars: 10 µm. **(G)** Polar plots of cilia orientation in the upper part of SP from P7 to P14. **(H)** The percentage of south-oriented cilia in the upper part of SP significantly increased from P7 to P14. One-way ANOVA with Bonferroni's multiple comparison test for **E & H**. **(I)** A schematic diagram depicting principal cell positioning and the reverse movement of centrioles/cilia of late-born neurons in the hippocampal CA1 region.

Fig. 4. Primary cilia directionality in the neocortex indicates a reverse movement of principal neurons during postnatal development. (A-B) Co-immunostaining of AC3, Arl13b and DAPI in Layer II and V at P3 and P7 from WT mice **(A)** and Arl13b+ mice **(B)**. Scale bars: 5 µm. (**C-D)** Quantification of cilia length in cortical Layer II and V. Primary cilia of early-born neurons were much longer than those of late-born neurons at P3 and P7 in both WT and Arl13b+ mice. Unpaired Student's T-test; *** $p < 0.001$, n = 3 mice, mix sex. **(E-H)** The densities of centrioles and nuclei in the superficial sublayer (Layer II/III) of the neocortex changed from compact and uneven at P3 to sparse and even at P14. The right two panels showing how top and middle sections were defined. Scale bars: 10 µm. **(F)** The ratios of centriole to nucleus (C/N ratio) in both top and bottom of the cortical superficial sublayer at P3 and P14 were all close

to 1. The density of nuclei **(G)** and centrioles **(H)** at P3 and P14 were quantified. Two-way ANOVA test with Bonferroni post hoc tests was applied in **(F-H)**. **(I)** The distance from the outer edge of Layer II to the pial surface, which is indicated in **(E)** by red arrows, increased significantly in the first two postnatal weeks. One-way ANOVA test with Bonferroni post hoc tests. (**J-K**) Primary cilia in both the superficial sublayer (Layer II/III) and deep sublayer (Layer V) in the neocortex orientated towards the pial surface. P14 and P40 in WT **(J)** and Arl13b+ **(K)** mice. Scale bars: 10 µm.

Fig. 5. CFSE tracing shows the reverse movement of late-born neocortical principal neurons during postnatal development. (A-B) CFSE neuron tracing shows that principal cells underwent a reverse movement during early postnatal stage. **(A)** CFSE dye expression pattern at P1, P3, P9 stayed at the injection site, the outermost layer of the superficial sublayer, while at P3, CFSE-labeled superficial sublayer cells appeared in the inner part layer, and further inside of the cortex at P9. Scale bar: 100 µm. **(B)** White boxes in **(A)** are enlarged. Scale bar: 20 µm. **(C-D)** CFSE-labeled migrating cells were ~70% Ctip2-positive cells, indicating that those migrating cells were principal cells. Scale bar: 10 µm. **(E)** Control: little lateral diffusion was observed at P1 and P9 when CFSE was injected into neocortical inner layers at P 0.5. Scale bars: 100 µm.

Fig. 6. Alterations of primary cilia function affects brain volume and neuronal number. (A) X-ray micro-CT of Ift88 flox/flox Emx1-Cre conditional knockout (Ift88 cKO) mice and controls at P20, scale bar: 1 mm. RSG: granular retrosplenial cortex area. An arrow indicates a gyrification site. **(B)** Thickness of different subregions of neocortex were quantified. One-way ANOVA with Bonferroni post hoc tests. **(C)** Ift88 cKO mice displayed significantly larger brain size after P5 than controls. One-way ANOVA with Bonferroni post hoc tests. **(D)** Ift88 cKO mice exhibited lower survival rate than controls (n = 20). **(E)** Arl13b flox/flox Emx1-Cre conditional knockout mice (Arl13b cKO) mice had a slightly larger brain at P9, but not at other ages. One-way ANOVA with Bonferroni post hoc tests was used. **(F)** Arl13b+ mice

exhibited significantly smaller brain size after P14 than control littermates (n = 4). Two-way ANOVA with Bonferroni post hoc tests. (**G-I**) Altered neuronal composition in neocortical lamina in Ift88 cKO mice. **(G)** Brain sections of Ift88 cKO and control mice at different ages were stained with Satb2 and Ctip2. Representative images of Layer V are shown. (**H**) Ift88 cKO mice had more Satb2-positive neurons (relative to nucleus counts) in Layer V from P5 to adulthood, but not before at P0 and P3. (**I**) There were no significant differences in Ctip2-positive neurons in Layer V between Ift88 cKO and control mice from P0 to adulthood.

Fig. 7. Selective ablation of primary cilia in the forebrain leads to gyrification in the retrosplenial cortex that occurs postnatally and is formed by reverse movement. (A-B) Ift88 cKO mice started to show a very shallow sulcus at E18.5 in the retrosplenial cortex, and the depth of sulcus increased drastically from P0 to P9, and then stabilized after P9. Scale bar: 100 µm. **(C)** Statistical data: the distances from the midline to the edge of the superficial sublayer or gyrification site. **(D)** Immunostaining using Ctip2 from P0 to P20 in the retrosplenial cortex of WT mice. White line represents the perpendicular distance from the brain midline to the edge of deep sublayer site in the retrosplenial cortex (marked by Ctip2), which were quantified in **(E)**. Scale bar: 100 µm.

Fig. 8. Selective disruptions of primary cilia function in the forebrain lead to altered CA1 lamination. (**A**) Co-immunofluorescence staining using Satb2 (red), Ctip2 (green) and DAPI (bule) on P5 control and Ift88 cKO mice. Ift88 cKO mice show significant difference in the distal CA1 at P5. Scale bar: 100 µm. (**B**) CA1 SP thickness naturally decreased with age in controls (top), Ift88 cKO mice exhibited delayed lamina condensation (bottom) and misplacement of cells in the 10 µm thickness CA1 SP. Scale bar: 10 µm. (**C**) Quantification of CA1 thickness from different ages. n = 3, total 9 regions total were quantified, Two-way ANOVA with Bonferroni post hoc tests. **(D)** Thickness quantification of the distal and proximal in CA1 SP at P5. n = 3, total 9 regions total were quantified. (**E**) Cilia were ablated in CA1 regions of

Ift88 cKO mice and shortened in Arl13b cKO mice. Scale bar: 10 µm. (**F**) Disruption of cilia function caused loosened distribution of principal neurons in CA1 SP (indicated by white arrows). Scale bars: 10 µm.

Fig. 9. Disruption of primary cilia function causes neuronal misplacement in DG. (**A**) representative images of AC3-labeled primary cilia in the granular cell layer. Centrioles were marked by Centrin2-GFP. The right panel is enlarged. Scale bar: 10 µm. **(B)** Polar plot of primary cilia orientation in DG. (**C**) Arl13b-labeled primary cilia were more prevalent at P9, while AC3-labled primary cilia were more abundantly expressed at P20 in the granular cell layer. Scale bar: 10 µm. (**D-G**) Cilia alterations led to misplaced neurons in DG. (**D**) Primary cilia were ablated in Ift88 cKO mice and shortened in Arl13b cKO mice. Scale bar: 10 µm. (**E**) Ift88 cKO and Arl13b cKO mice lost the compactness of the granular cell layer. Both coronal and sagittal sections show similar patterns. Scale bar: 100 µm. (**F**) A diagram depicting the quantification method of misplaced neurons in the outer molecular layer of DG. (**G**) Quantification results of misplaced neurons in DG of coronal sections (left) and sagittal sections (right). Two-way ANOVA with Bonferroni post hoc tests were used for statistical analysis.

Supplemental Figures:

Fig. S1. Allen Brain Atlas *in situ* hybridization staining of Ndst4 over ages, Col11a1 and Htr1a at P56 in mouse hippocampal CA1. The thickness of CA1 SP continued to decrease with age. The mRNA of Ndst4, a deep sublayer marker gene[25], was mostly expressed in the deep sublayer of CA1 SP, but the distribution was dynamic with age. M: month. These images also demonstrate early- and late-born neuronal distribution in CA1 SP. Images having same scale bars were adopted from Allen Brain Atlas (https://mouse.brain-map.org/).

Fig. S2. Strong regulation of CA1 neuronal cilia length by Arl13b. (A-B) Arl13b+ mice in C57Bl/6J background had much longer neuronal primary cilia than WT mice in the hippocampal subregions (CA1, CA3 and DG) in adults. Notably, CA1 region had the longest primary cilia and the effect of Arl13b on promoting cilia length is very strong. Compared with WT mice, the average CA1 cilia length increase by over 60% in Arl13b+ mice. **(C-D)** Compared to hippocampal regions, primary cilia length was not strongly changed in other brain regions such as neocortex and amygdale. Immunostaining of neuronal primary cilia in WT controls and Arl13b overexpression transgenic (Arl13b+) mice. Unpaired Student's T-test was applied in (**B** and **D**). Scale bar: 10 μm. Data were collected from at least 3 young adult mice for each genotype. Mix sex.

Fig. S3. Neuronal ciliation coincides with maturation in CA1 SP. (A) at P3, Early-born neurons in the deep sublayer protruded cilia earlier than neurons in the superficial sublayers of the CA1 in Arl13b+ mice, and those early-protruding cilia pointed north. **(B)** NeuN expression was first detected in deep-sublayer of SP at P1, more at P5, then extended to superficial-layer neurons at P7. At P14, both deep- and superficial-layer neurons had abundant NeuN expression. Scale bars: 10 μm. **(C)** Allen Brain Atlas in situ hybridization (ISH) results of Shank3, a synaptic maker of excitatory neurons, in hippocampal CA1 at P4 and P14. At P4, Shank3 was only expressed in the deep sublayer of SP and Layer V (deep sublayer) of the neocortex. At P14, ISH signals of this gene were presented in most areas of SP and the six layers in the neocortex. Scale bars: 100 μm. **(D)** NeuN staining in the postnatal neocortex. Principal neurons in outer layer of the neocortex are not matured at P3. In addition, NeuN expression abundance display a decreasing gradient from the deep to superficial layers, even neuron numbers increase.

Fig. S4. The primary cilia of early- and late-born neurons in the ventral hippocampal CA1 region clearly display opposite directionality. Representative images of primary cilia in the ventral CA1 regions at P9. Top Left panels are enlarged images at P9. Data from WT brain sections were strained with

AC3 and Arl13b antibodies. Arl13b+ primary cilia and centrioles were marked by Arl13b-mCherry and Centrin2-GFP, respectively. Bottom panels are polar plots of primary cilia orientations of WT and Arl13b+ at P9 and P40. Arrows indicate the changes of SO-pointing cilia orientations from P9 to P40.

Fig. S5. CA3 neurons mature and protrude cilia earlier than CA1 neurons. (**A-C**) Neuronal primary cilia were abundantly expressed in the CA3 region of both WT and Arl13b+ mice at P5 and P7. NeuN expression in CA3 at P5 (A) was also stronger. Scale bars: 10 µm. (**D**) CA3 pyramidal neurons matured earlier than CA1 neurons. At P4, CamK2a, a postsynaptic marker protein, was highly and widely expressed throughout the CA3. In contrast, its expression was only restricted to the deep sublayer of CA1, not yet present in the superficial sublayer. Scale bars: 100 µm. ISH images were adopted from the Allen Brain Atlas Developing Mouse Brain. (**E**) Primary cilia directionality in the CA3 region of Arl13b+ is different from the CA1. Confocal imaging was collected from Arl13b+ mice. Polar plot and histogram show primary cilia orientation in the CA3 region.

Fig. S6. Only principal neurons in laminated brain regions exhibit specific cilia directionality. (A) Immunostaining of primary cilia in different brain regions including subiculum, thalamus, hypothalamus, neocortex, and cingulate cortex. Scale bar: 10 µm. **(B)** A diagram summarizing the orientation of neuronal primary cilia in multiple brain subregions. **(C-G)** Primary cilia of interneurons and astrocytes do not display specific directionality. **(C)** Interneurons' primary cilia do not point in specific directions. Straining using Ift88 flox/flox Camk2a-Cre (T-29) P20 sections shows remaining primary cilia of interneurons in the hippocampal CA1 and neighboring neocortex. Because AC3 is a marker for neuronal primary cilia and the Camk2a-Cre strain has Cre expression selectively in forebrain principal neurons, primary cilia marked by AC3 in Ift88 flox/flox Camk2a-Cre belong to interneurons. **(D)** Astrocytic primary cilia in the hippocampus, denoted by white arrows, did not exhibit specific directionality. (**E**) Astrocytic primary cilia in the neocortex did not exhibit specific directionality. Two representative images are shown. White

arrows denote astrocyte cilia, which display irregular pointing. Green arrows denote neuronal primary cilia, which point in the pia direction. (**F-G**) Polar plots of astrocytic primary cilia orientation in the hippocampus (**F**) and neocortex (**G**). (**D-G)** data were collected from Arl13b-mCherry brain sections that were stained by Arl13b and GFAP antibodies.

Fig. S7. The changes in ratios of neocortical layers during postnatal development are indicative of inward migration. (A) Cortical co-immunofluorescence staining using Satb2 and Ctip2 antibodies. White line indicates whole six layers of the neocortex; red line labels the neocortical superficial sublayer starting from the top edge of Layer V to the pial surface; green line marks Layer VI starting from the bottom edge of layer V to the end of Ctip2 expression. Scale bar: 100 µm. **(B)** The ratio of superficial sublayer to whole 6 layers increased after birth and stabilizes after P20. **(C)** The ratio of deep sublayer V to whole 6 layers decreased postnatally. **(D)** The ratio of Layer VI to whole 6 layers decreased significantly in the first week after birth and stabilized after P20. n=3, mix sex, one-way ANOVA with Bonferroni post hoc tests. **(E)** The distances from Layer VI to the ventricular zone (VZ) decreased over ages. Data of **(E**) were quantified based on red line between the VZ to the edge of Layer VI using Allen Brain Atlas images **(F**). Scale bars: 100 µm.

Fig. S8. Subiculum and postsubiculum exhibit a reverse movement for lamina refinement during postnatal development. (A) Ctip2 ISH staining from E18.5, P4 and P14 of mouse sagittal sections. Bule arrows denote the curvature between the postsubiculum that emerge at P4 and becomes remarkable at P14. Red arrows denote the demarcation between CA1 and subiculum, which becomes more obvious with age. **(B)** Similar pattern changes in the CA1, subiculum, postsubiculum and neocortex were observed in Etv1 ISH staining. Staining using other markers show similar departmental pattern. VZ: the ventricular and subventricular zone, Sub: subiculum, POST: postsubiculum. ISH Data were adopted from Allen Brain Atlas.

Fig. S9. Comparative anatomy of the mammalian hippocampi. Red arrows indicate compact superficial sublayers (Super.). Green arrows denote putative reverse direction of projection neurons. Sub: subiculum. Images of roe dear, jackal, and boar are modified from ref. 67 (Credit to Malikovic et al., Front Neuroanat 2022), mole rat image from ref. 46 (Credit to Radic et al., Front Neuroanat 2017), respectively. Original images are cropped, and we add arrows and texts denote the direction of reverse movement. The macaque image is from NIH Non-Human Primate Brain Atlas. In macaque, the pyramidal shape of CA1 neurons is in line with putative reverse direction (enlarged on the bottom). The sparsely layered CA1 SP of primates is likely formed via reverse movement of principal neurons from the condensed superficial layer to deep sublayer. Note that the CA3 and DG principal cell layers remain highly compact.

Fig. S10. A working model of principal cell positioning. A slow reverse movement of principal neurons is needed for configurating various inside-out laminae in the cerebral cortex spanning from the neocortex to the hippocampal CA1. In the neocortex and neighboring regions (the entorhinal and cingulate cortex), both early- and late-born neurons reverse. In the hippocampal CA1 SP or other allocortices, which are compact, late-born neurons reverse, whereas early-born neurons do not. Primary cilia of principal neurons indicate the direction of reverse movement. White and blue arrows indicate the direction of radial migration of principal cells (mostly during embryonic stage) and postnatal reverse movement, respectively. Deep: deep sublayer; Super.: superficial sublayer. VZ: the ventricular zone. The early-born and late-born neurons in the CA3 are not well separated. Additionally, DG lamina is formed by outside-in migration pattern. Thus, CA3 and DG do not fit this model.

Supplemental Tables:

Regions	CA1 -deep	CA1 -super.	Cortex -deep	Cortex -super.	CA3 -deep	CA3 -super.	DG-out¶	DG-in¶
Ciliation Time (WT)	P3-P7	P9-P10	P3-P7	P7-P10	P3-P7	P3-P7	P3-P7	After P7
Ciliation Time (Arl13B+)	P0-P7	P7-P10	P0-P7	P7-P10	P0-P7	P0-P7	P0-P7	After P7
Cilia Length (WT)	<1 µm, P7	<1 µm, P7	3.3±0.1 µm, P7	1.0±0.0 µm, P7	5.6±0.1 µm, Adult		2.3±0.0 µm, Adult	
	7.0±0.1 µm, Adult		5.6±0.1µm, Adult	5.0±0.0 µm, Adult				
Cilia Length (Arl13B+)	1.5±0.0 µm, P3	1.0±0.0 µm, P3	1.9±0.1 µm P3	0.7±0.0 µm P3	8.2±0.1 µm, Adult		3.1 ± 0.0 µm, Adult	
	4.5±0.1 µm, P7	2.8±0.1 µm, P7	4.5±0.1 µm P7	2.1±0.1 µm P7				
	11.7±0.1 µm, Adult		6.3±0.1 µm, Adult	5.3±0.0 µm, Adult				
Reverse movement	No	Yes	Yes	Yes	TBD			
NeuN# Expression	P3-P5	P7-P14	P0-P1	P5	P3-P5	P3-P5‡	P5-P7	P7-P10
Camk2a* Expression	~P4	P4-P14	~P4	P4-P14	~E18.5-P4	~E18.5-P4	P4	After P4
Shank3* Expression	~P4		~P4		~E18.5-P4	TBD		
Homer 1* Expression	~P4		~P4		~P4-P14	~P4-P14		
PSD-95* Expression	~P4 or earlier		~P4 or earlier		~E18.5-P4	~E18.5-P4		
Synapsin 1* Expression	~P4		~P4		~ E18.5-P4	~E18.5-P4		
Syntaxin1* Expression	~P4		~P4 or earlier		~ E18.5-P4	~ E18.5-P4	Not expressed	Not expressed

TBD: to be determined. Super., superficial sublayer. P: postnatal; E: embryonic. Adult: 2–4 months old. ¶ Dentate gyrus outer granular layer and inner granular layer. † CA3 deep-superficial distinction in ciliation and neuronal maturation is not as obvious as CA1. ? Require further verification. ‡ CA3 pyramidal neurons mature several days earlier than CA1 neurons. # Based on our immunostaining data using anti-NeuN antibody. ƒ Outmost superficial layer in the neocortex * Based on ISH data from the Allen Brain Atlas Developing Mouse Brain.

Table S1. Features of neuronal primary cilia and neuronal maturation in hippocampal subregions and the neocortex.

Brain Regions or Cell Types	Primary Cilia Directionality	Cell Density in Lamina
DG	Opposite	Compact
Dorsal CA1	Opposite	Compact
Ventral CA1	Opposite	Compact
Olfactory Tubercle	Opposite	Compact
Piriform Cortex (Layer II)	Opposite	Compact
Piriform Cortex (Layer III)	Same, to the pia	Loose
Neocortex	Same, orientate towards the pia	Loose
Cingulate Cortex	Same, to the pia	Loose
Entorhinal Cortex	Same, to the pia	Loose
Subiculum	Same, to the pia	Loose
Postsubiculum	Same, to the pia	Loose
CA1 Interneurons	Irregular	Not layered
CA1 Astrocytes	Irregular	Not layered
Neocortex Astrocytes	Irregular	Not layered
Thalamus	Irregular	Not layered
Hypothalamus	Irregular	Not layered
Amygdala	Irregular	Not layered
Striatum	Irregular	Not layered

Table S2. Primary cilia directionality in different brain regions or cell types, in association with cell density and lamination. Primary cilia orientation of principal neurons may change to some degree with age. The best timing to measure cilia directionality of principle neurons is at P14-P20 when principal neurons have completed cell positioning.

Cortical Regions		Speed (µm/hr)	Distance (µm)	Estimation Methods	Outcomes
Dentate Gyrus (outside-in)		ND	ND	Cilia orientation perpendicular to lamina	Lamina compact across all mammalian species
CA1-SP (mice)	Deep	No	No	Centriole position unchanged and cilia orientate toward ventricular zone	SP gradually becomes compact and narrow
	Super.	0.1-0.2	10-35	Centriole movement and SP lamina thickness change	
CA1-SP (Monkeys)		ND	ND	Cilia orientate towards the pia	SP becomes loose layered
CA3-SP (mice)	Deep	*Unclear*	*Unclear*	Early- and late-born neurons highly mingled, unable to estimate reverse speed	Deep-superficial lamination in CA3 SP different from CA1 SP
	Super.				
Subiculum*		0.2-0.3	30-200	Lamina upward shift and expansion, cilia orientation	Generate a sparse lamina distinct from CA1 SP
Postsubiculum*		0.2-1	100-300	Laminae backward shift and expansion, cilia orientation	Form sparse laminae with inward curvature
Neocortex	Super.	1-3	up to 600	Neuron tracing by CFSE dye, principal neuron cilia directionality	Laminae become sparse and even;
	Deep*	0.5-2	200-400	Layer VI to VZ distance change	
Retrosplenial cortex (cingulate cortex, WT)		0.3-0.6	100-300	Postnatal changes in Layer I-VI	Layer I expand and Layer II-VI principal neurons move inward
Retrosplenial cortex (Ift88 lox/lox Emx1-cre mice)		0.8-1.2	200-400	Postnatal changes in gyrification	Develop gyrification
Claustrum[§]		*5.2±0.6*	*ND*	*Oshima et al., 2023 J. Neurosci[79].*	Form claustrum
Developing Neocortex *"Multipolar migration"*		*1.6-6.4*	*ND*	*Tabata et al., 2003 J. Neurosci[68].*	Forward migration to form the outer layer of principal neurons
Developing Neocortex *"Radial migration"*		*9-12 or 38.6±4.7*	*ND*	*Tabata et al., 2003 J. Neurosci[68].* *Borrell et al., 2006 Cerebral Cortex[80].*	

No: No reverse movement. * Estimation based on my own imaging data and Allen Brain Atlas. VZ: the ventricular zone. [§] This reverse movement occurs during the embryonic stage and has a higher speed. ND: not determined

Table S3. Features of reverse movement and its impacts on laminar structures in the cerebral cortex. The speeds of reverse movement are a rough estimation, detailed assays are needed to precisely determine the reverse speeds in different layers. The distances of backwards movement vary from 10-35 µm in the CA1 up to 600 µm in the neocortex of mice.

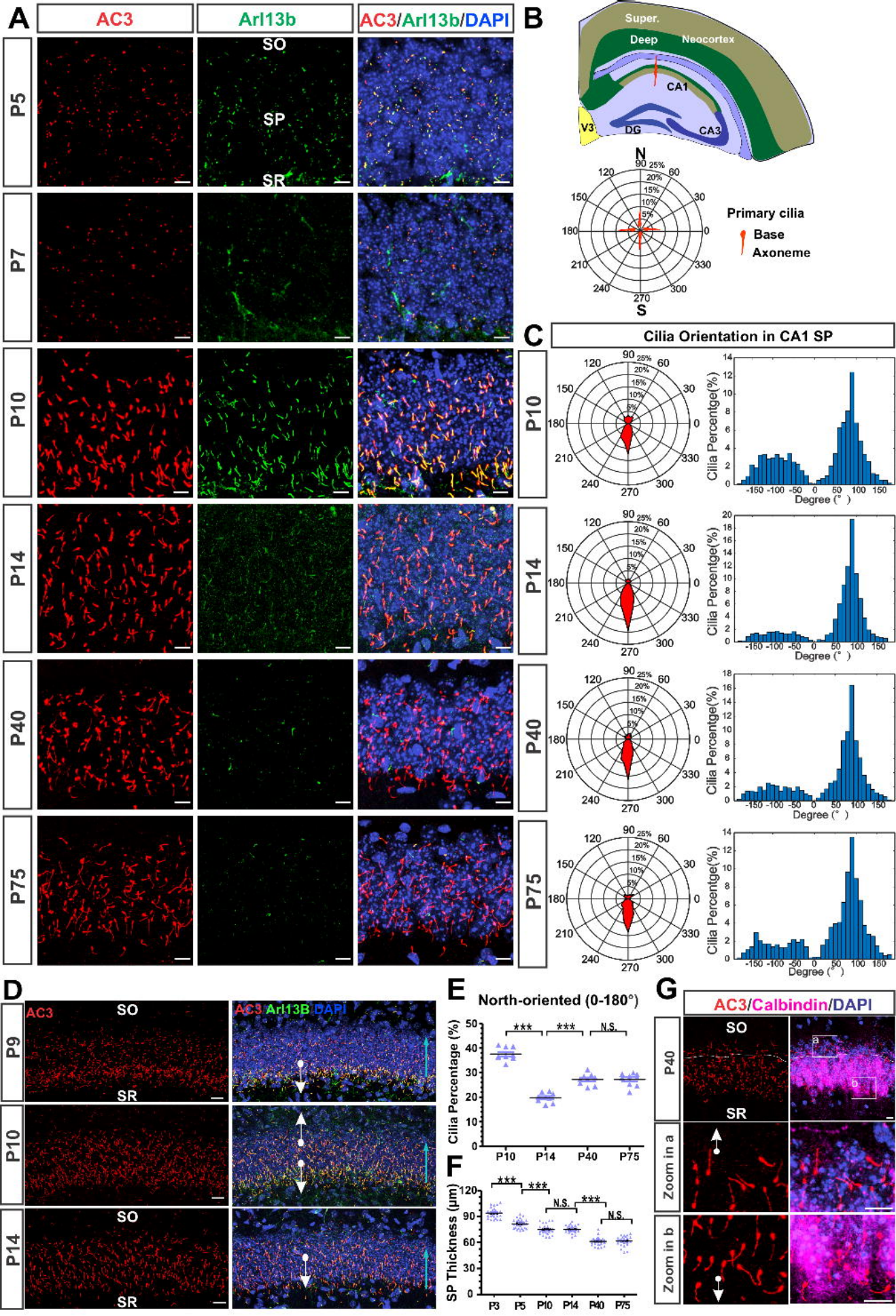
A
AC3
Arl13b
AC3/Arl13b/DAPI
P5
P7
P10
P14
P40
P75
SO
SP
SR
B
Super.
Deep
Neocortex
CA1
V3
DG
CA3
N
S
Primary cilia
Base
Axoneme
C
Cilia Orientation in CA1 SP
Cilia Percentge(%)
Degree (°)
D
AC3
AC3 Arl13B DAPI
P9
P10
P14
E
North-oriented (0-180°)
Cilia Percentage (%)
N.S.
F
SP Thickness (μm)
P3
P5
P10
P14
P40
P75
G
AC3/Calbindin/DAPI
Zoom in a
Zoom in b

Figure 1

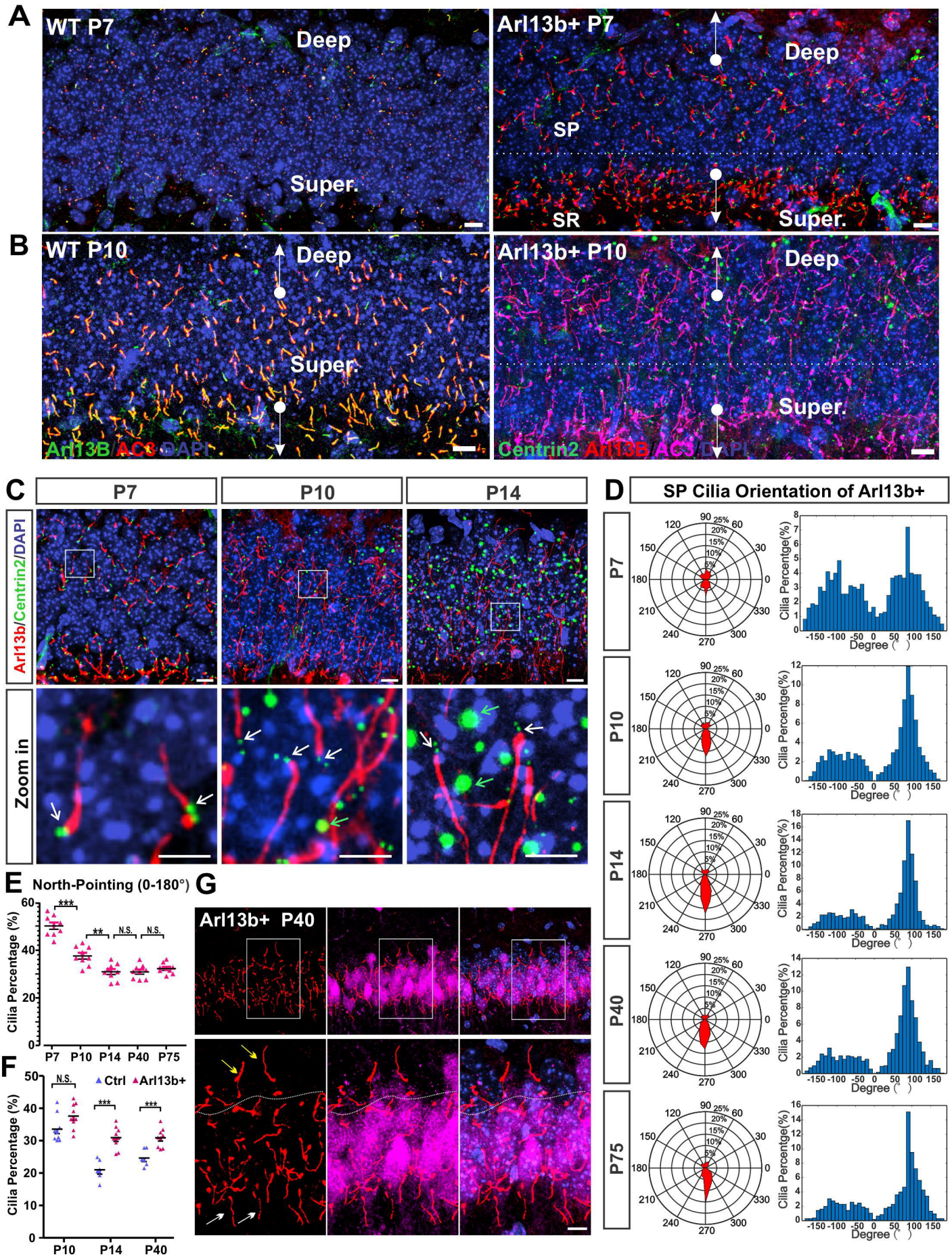
A
WT P7
Deep
Super.
Arl13b+ P7
Deep
SP
SR
Super.
B
WT P10
Deep
Super.
Arl13B/AC3/DAPI
Arl13b+ P10
Deep
Super.
Centrin2/Arl13B/AC3/DAPI
C
P7
P10
P14
Arl13b/Centrin2/DAPI
Zoom in
D
SP Cilia Orientation of Arl13b+
P7
P10
P14
P40
P75
Cilia Percentge(%)
Degree (°)
E
North-Pointing (0-180°)
Cilia Percentage (%)
P7
P10
P14
P40
P75
***
**
N.S.
N.S.
F
Ctrl
Arl13b+
N.S.
***
***
Cilia Percentage (%)
P10
P14
P40
G
Arl13b+ P40

Figure 2

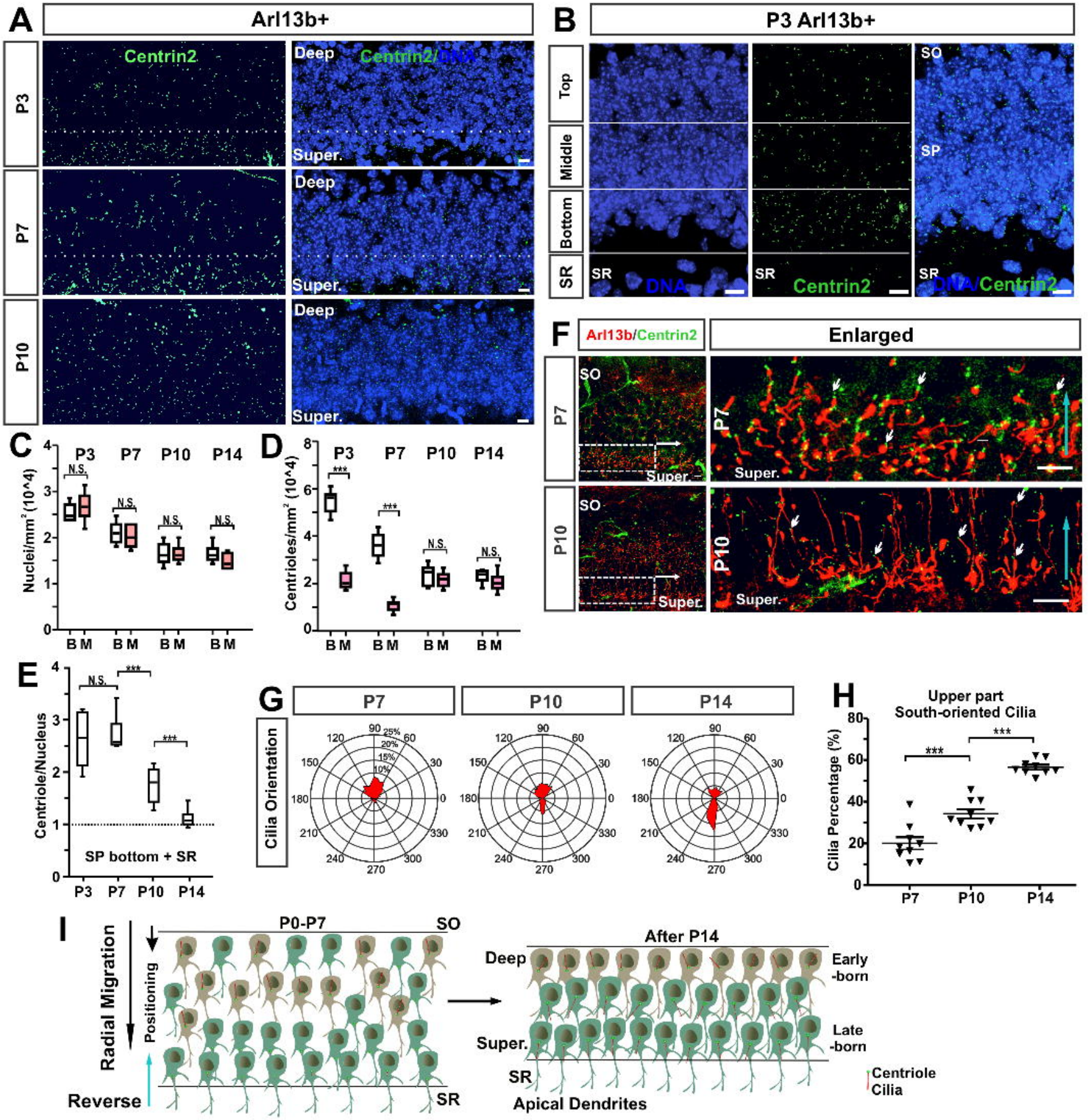
A
Arl13b+
P3
P7
P10
Centrin2
Deep
Centrin2/DNA
Super.
B
P3 Arl13b+
Top
Middle
Bottom
SR
SO
SP
DNA
Centrin2
DNA/Centrin2
C
Nuclei/mm² (10^4)
P3
P7
P10
P14
N.S.
B M
D
Centrioles/mm² (10^4)
***
E
Centriole/Nucleus
SP bottom + SR
F
Arl13b/Centrin2
Enlarged
G
Cilia Orientation
H
Upper part
South-oriented Cilia
Cilia Percentage (%)
I
P0-P7
Radial Migration
Positioning
Reverse
After P14
Deep
Early -born
Super.
Late -born
Apical Dendrites
Centriole
Cilia

Figure 3

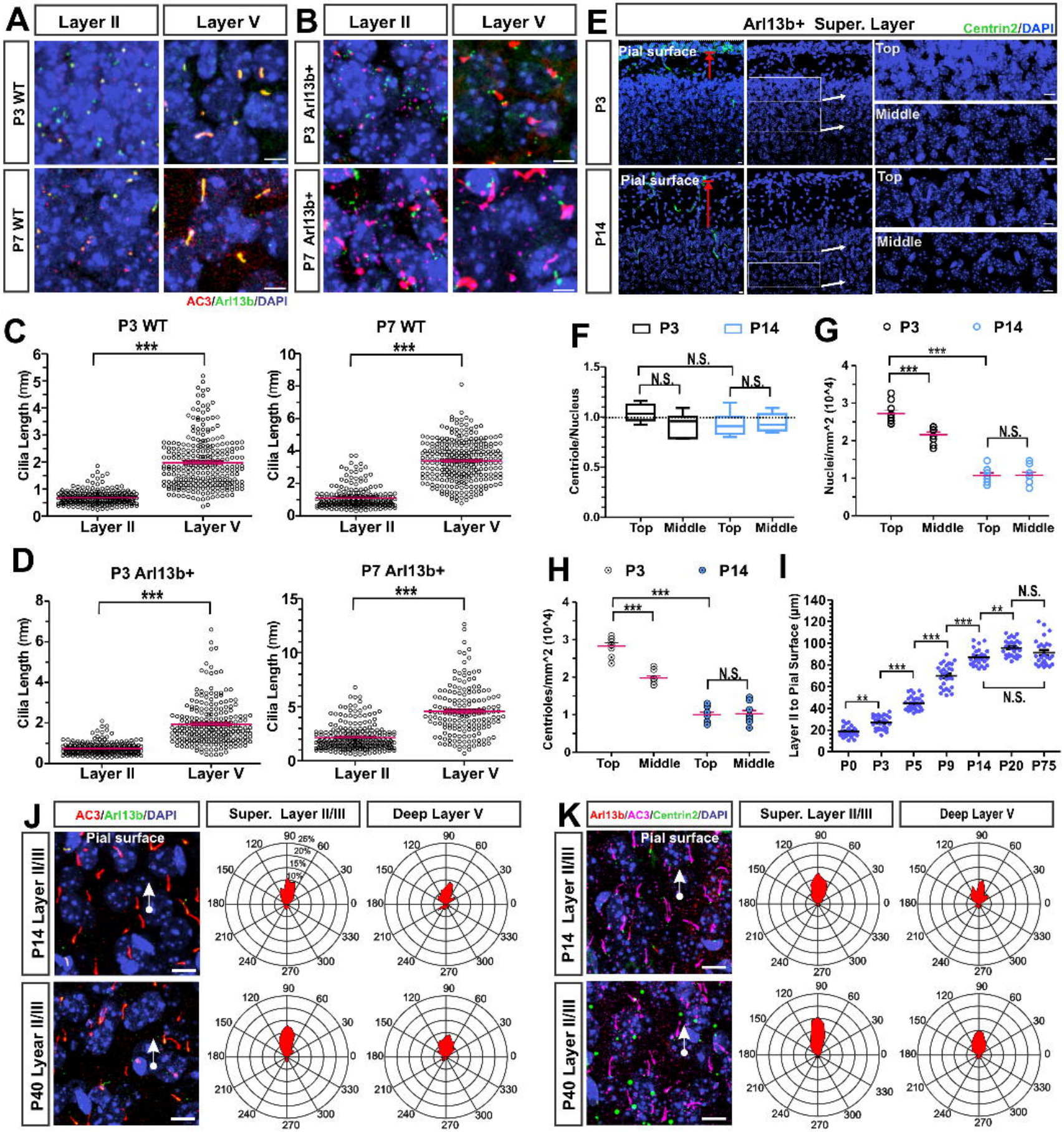
A
Layer II
Layer V
P3 WT
P7 WT
AC3/Arl13b/DAPI
B
P3 Arl13b+
P7 Arl13b+
E
Arl13b+ Super. Layer
Centrin2/DAPI
Pial surface
Top
Middle
P3
P14
C
P3 WT
P7 WT
Cilia Length (mm)
***
D
P3 Arl13b+
P7 Arl13b+
F
P3
P14
Centriole/Nucleus
N.S.
G
Nuclei/mm^2 (10^4)
H
Centrioles/mm^2 (10^4)
I
Layer II to Pial Surface (µm)
P0
P3
P5
P9
P14
P20
P75
J
AC3/Arl13b/DAPI
Super. Layer II/III
Deep Layer V
P14 Layer II/III
P40 Lyear II/III
K
Arl13b/AC3/Centrin2/DAPI
P14 Layer II/III
P40 Layer II/III

Figure 4

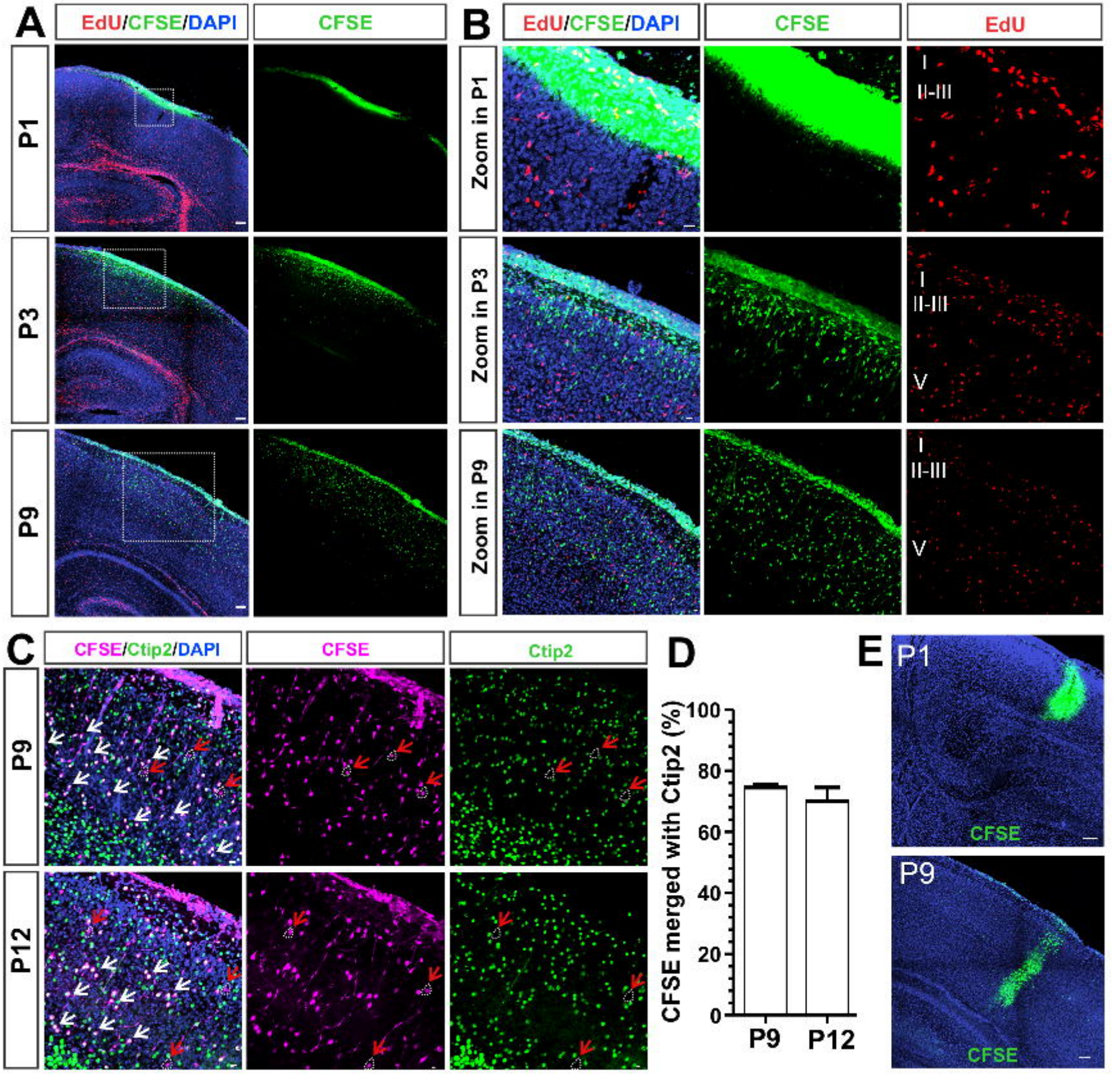
A
EdU/CFSE/DAPI
CFSE
P1
P3
P9
B
EdU/CFSE/DAPI
CFSE
EdU
Zoom in P1
Zoom in P3
Zoom in P9
I
II-III
V
C
CFSE/Ctip2/DAPI
CFSE
Ctip2
P9
P12
D
CFSE merged with Ctip2 (%)
100
80
60
40
20
0
P9
P12
E
P1
CFSE
P9
CFSE

Figure 5

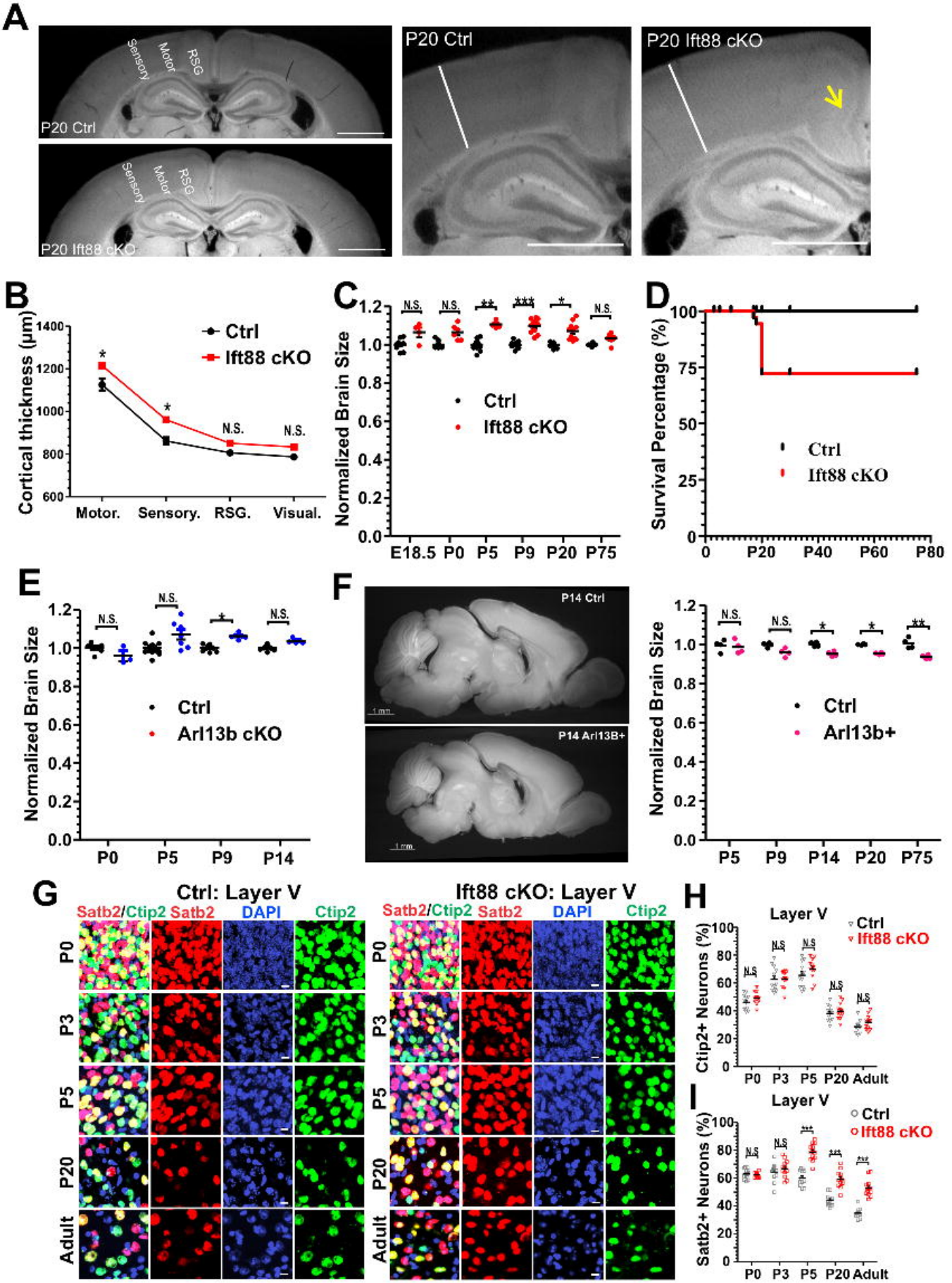
A
Sensory
Motor
RSG
P20 Ctrl
P20 Ift88 cKO
B
Cortical thickness (μm)
Ctrl
Ift88 cKO
Motor.
Sensory.
RSG.
Visual.
C
Normalized Brain Size
E18.5
P0
P5
P9
P20
P75
D
Survival Percentage (%)
E
Arl13b cKO
F
P14 Ctrl
P14 Arl13B+
Arl13b+
G
Ctrl: Layer V
Ift88 cKO: Layer V
Satb2/Ctip2
Satb2
DAPI
Ctip2
Adult
H
Layer V
Ctip2+ Neurons (%)
I
Satb2+ Neurons (%)

Figure 6

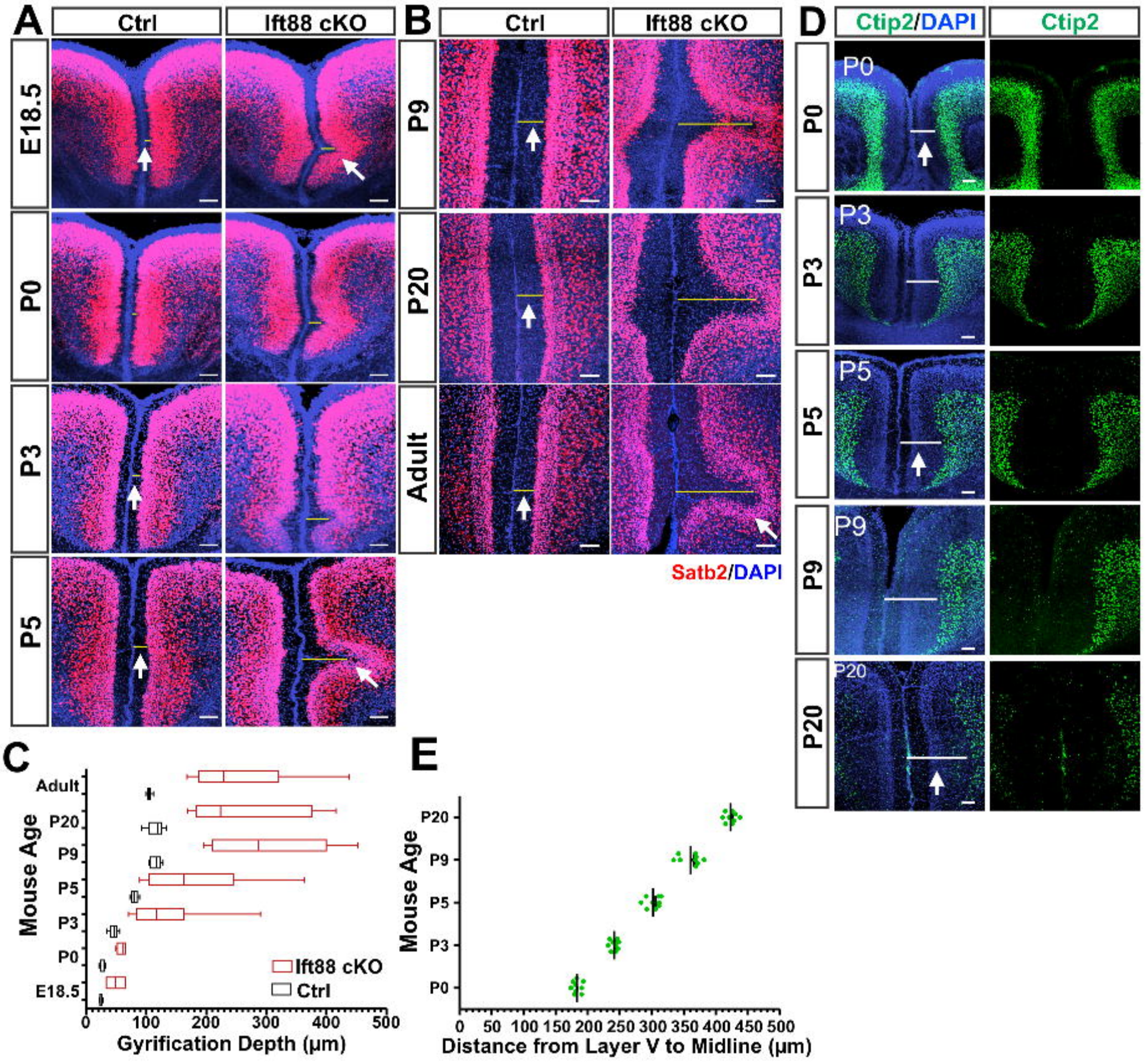
A
Ctrl
Ift88 cKO
E18.5
P0
P3
P5
B
Ctrl
Ift88 cKO
P9
P20
Adult
Satb2/DAPI
D
Ctip2/DAPI
Ctip2
P0
P3
P5
P9
P20
C
Mouse Age
Adult
P20
P9
P5
P3
P0
E18.5
Ift88 cKO
Ctrl
0
100
200
300
400
500
Gyrification Depth (μm)
E
Mouse Age
P20
P9
P5
P3
P0
0 50 100 150 200 250 300 350 400 450 500
Distance from Layer V to Midline (μm)

Figure 7

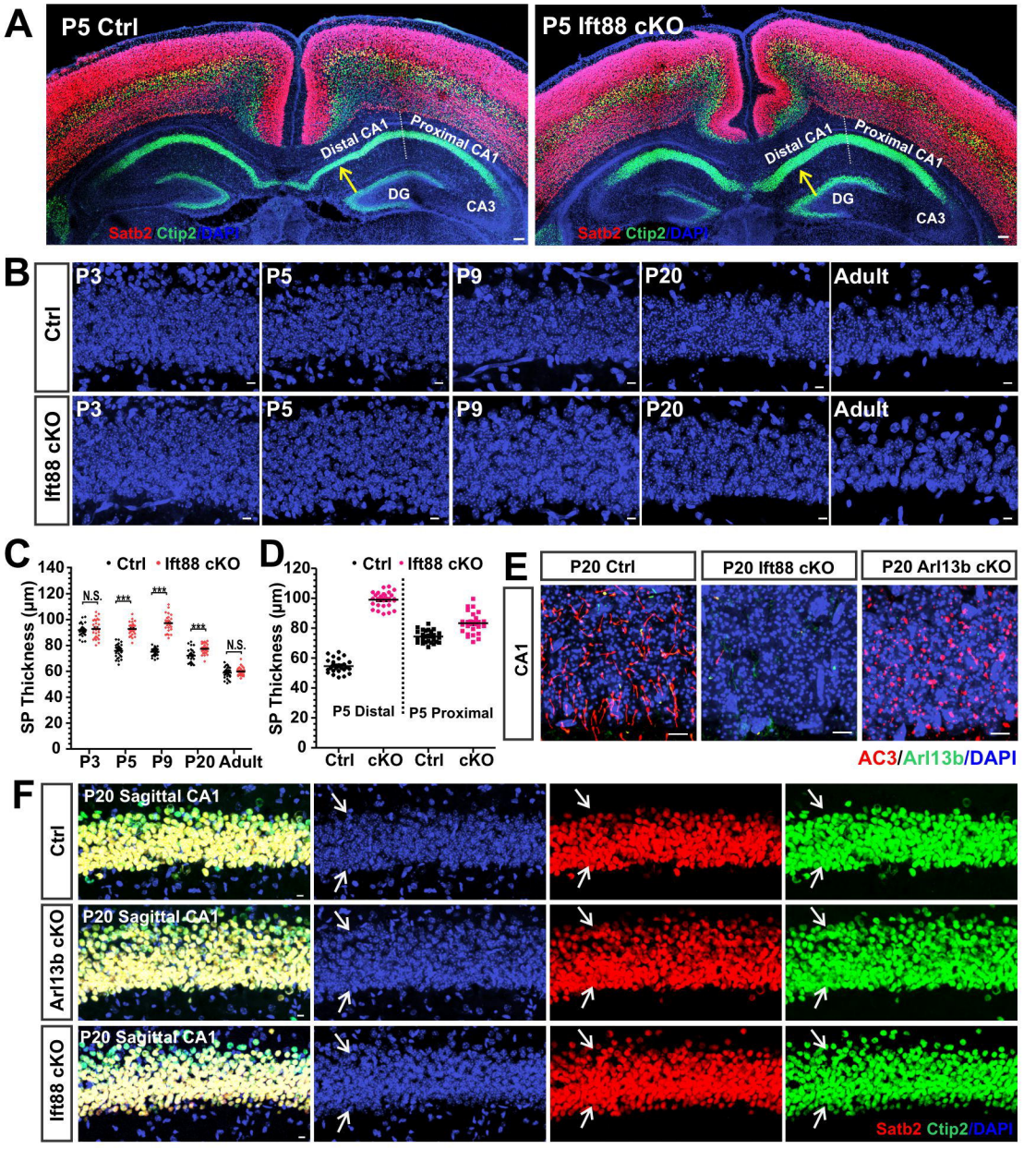
A
P5 Ctrl
P5 Ift88 cKO
Distal CA1
Proximal CA1
DG
CA3
Satb2/Ctip2/DAPI
B
Ctrl
Ift88 cKO
P3
P5
P9
P20
Adult
C
Ctrl
Ift88 cKO
SP Thickness (μm)
N.S.
***
P3
P5
P9
P20
Adult
D
Ctrl
Ift88 cKO
SP Thickness (μm)
P5 Distal
P5 Proximal
Ctrl
cKO
Ctrl
cKO
E
P20 Ctrl
P20 Ift88 cKO
P20 Arl13b cKO
CA1
AC3/Arl13b/DAPI
F
Ctrl
Arl13b cKO
Ift88 cKO
P20 Sagittal CA1
Satb2/Ctip2/DAPI

Figure 8

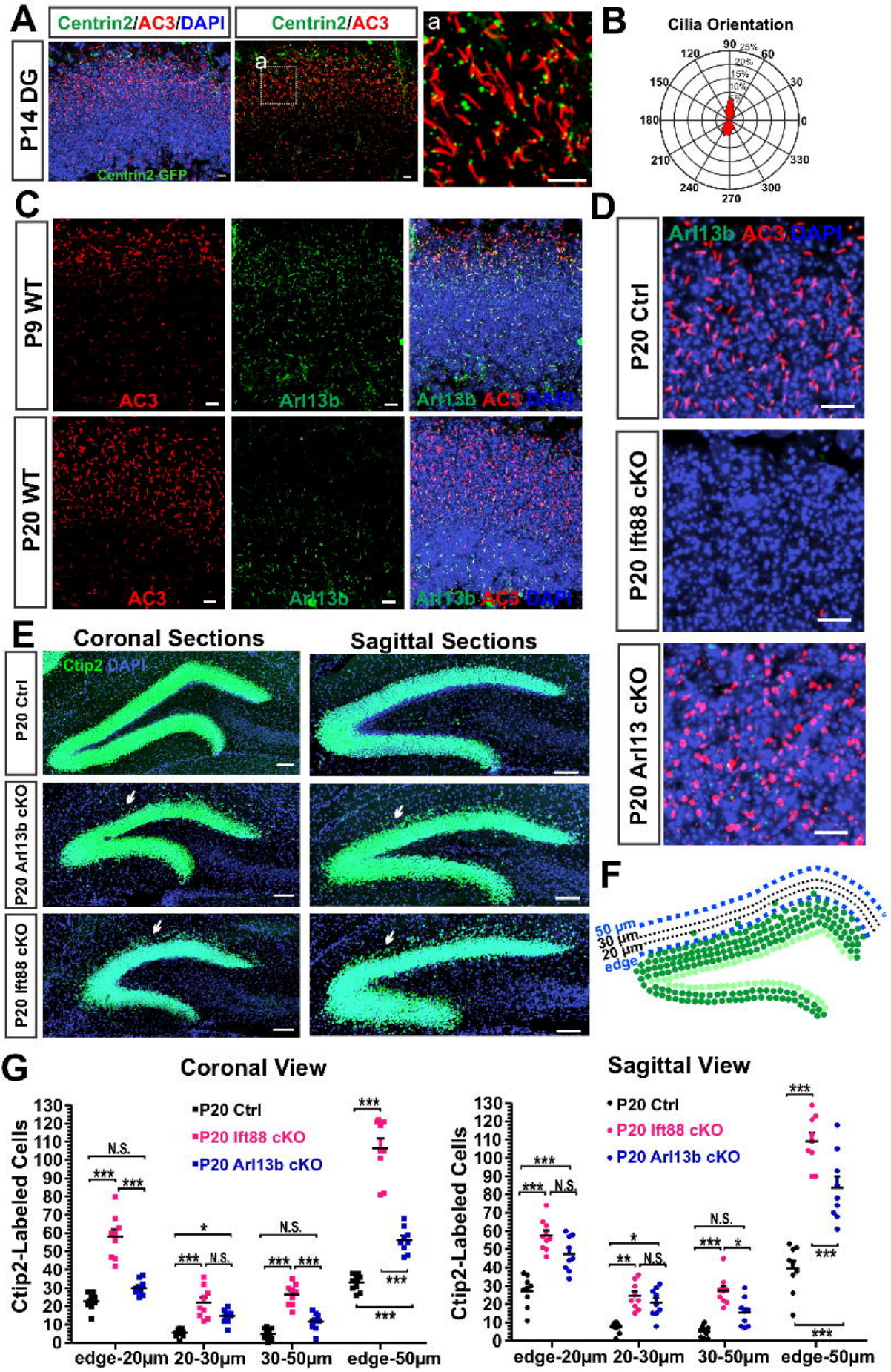
A
Centrin2/AC3/DAPI
Centrin2/AC3
P14 DG
Centrin2-GFP
a
B
Cilia Orientation
C
P9 WT
P20 WT
AC3
Arl13b
Arl13b AC3 DAPI
D
P20 Ctrl
P20 Ift88 cKO
P20 Arl13 cKO
E
Coronal Sections
Sagittal Sections
Ctip2 DAPI
P20 Ctrl
P20 Arl13b cKO
P20 Ift88 cKO
F
50 µm
30 µm
20 µm
edge
G
Coronal View
Sagittal View
Ctip2-Labeled Cells
P20 Ctrl
P20 Ift88 cKO
P20 Arl13b cKO
edge-20µm
20-30µm
30-50µm
edge-50µm
N.S.

Figure 9

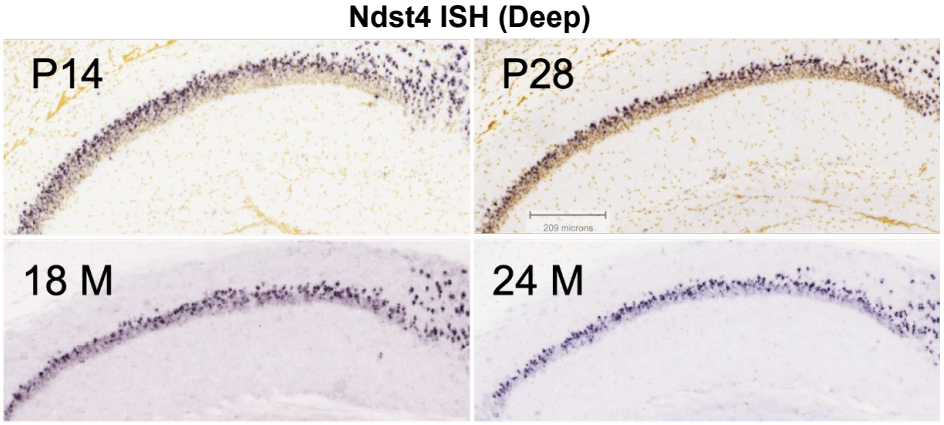

Figure S1

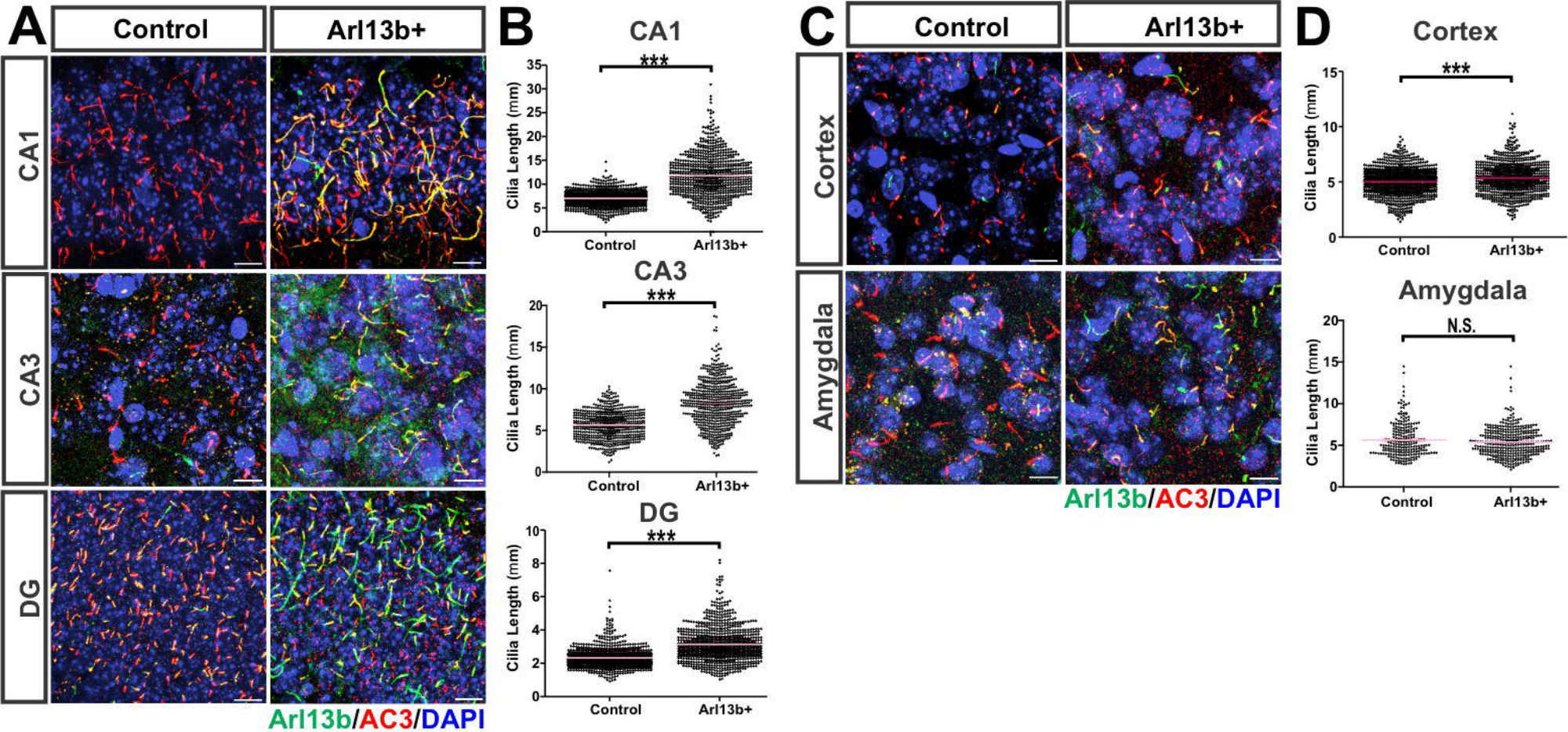
A
Control
Arl13b+
CA1
CA3
DG
Arl13b/AC3/DAPI
B
CA1
***
Cilia Length (mm)
Control
Arl13b+
CA3
***
Cilia Length (mm)
Control
Arl13b+
DG
***
Cilia Length (mm)
Control
Arl13b+
C
Control
Arl13b+
Cortex
Amygdala
Arl13b/AC3/DAPI
D
Cortex
***
Cilia Length (mm)
Control
Arl13b+
Amygdala
N.S.
Cilia Length (mm)
Control
Arl13b+

Figure S2

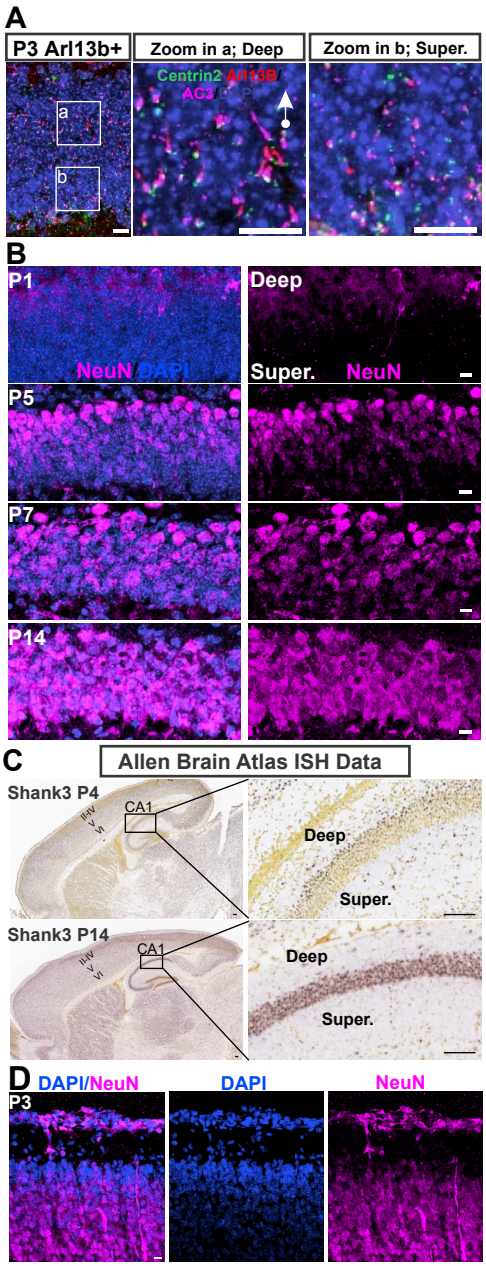
A
P3 Arl13b+
Zoom in a; Deep
Zoom in b; Super.
a
b
Centrin2 Arl13B
AC3 DAPI
B
P1
NeuN/DAPI
Deep
Super.
NeuN
P5
P7
P14
C
Allen Brain Atlas ISH Data
Shank3 P4
CA1
Deep
Super.
Shank3 P14
CA1
Deep
Super.
D
DAPI/NeuN
DAPI
NeuN
P3

Figure S3

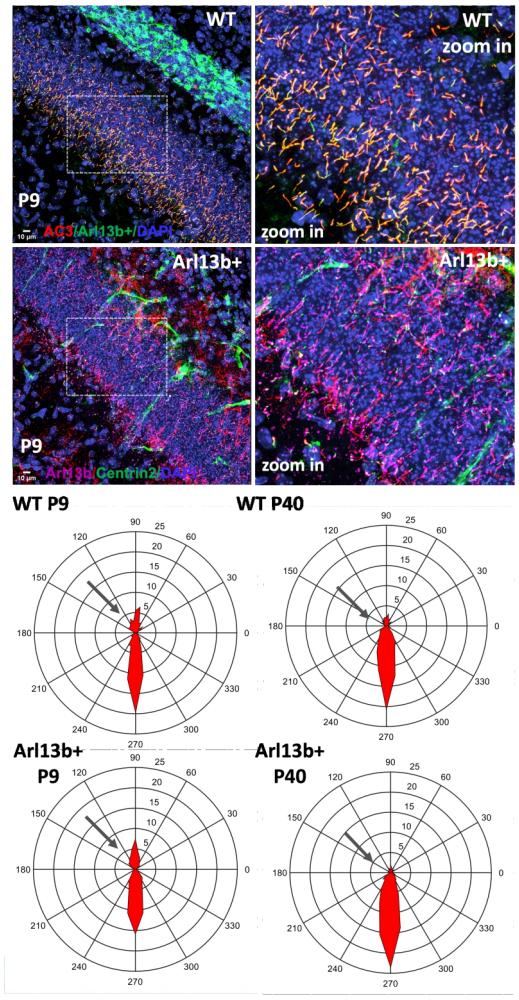
WT
WT
zoom in
P9
AC3/Arl13b+/DAPI
zoom in
Arl13b+
Arl13b+
P9
Arl13b/Centrin2/DAPI
zoom in
WT P9
WT P40
Arl13b+
P9
Arl13b+
P40

Figure S4

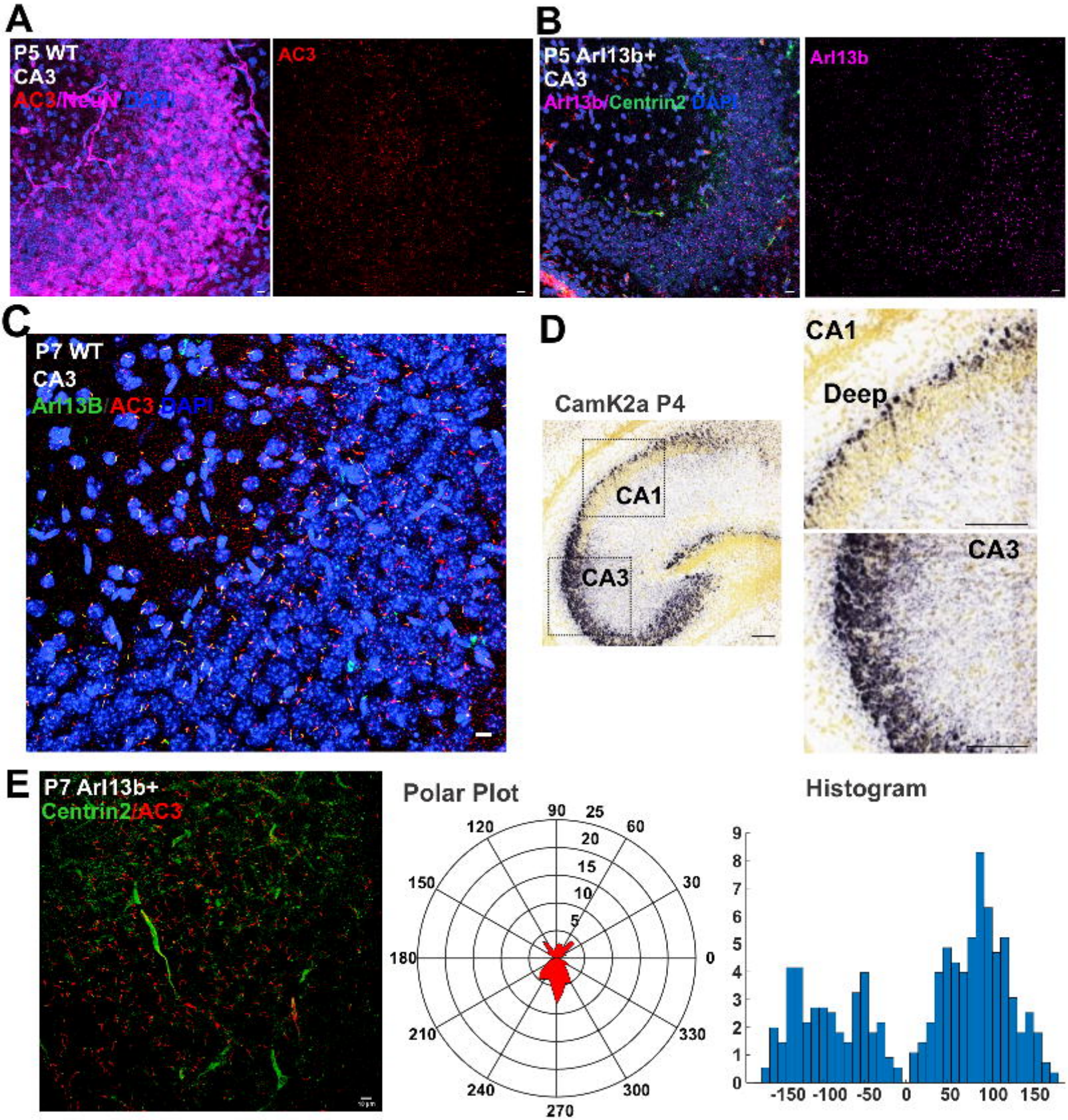
A
P5 WT
CA3
AC3/NeuN/DAPI
AC3
B
P5 Arl13b+
CA3
Arl13b/Centrin2/DAPI
Arl13b
C
P7 WT
CA3
Arl13B/AC3/DAPI
D
CamK2a P4
CA1
CA3
CA1
Deep
CA3
E
P7 Arl13b+
Centrin2/AC3
Polar Plot
90
25
60
20
15
10
5
120
30
150
180
0
210
330
240
300
270
Histogram
9
8
7
6
5
4
3
2
1
0
-150 -100 -50 0 50 100 150

Figure S5

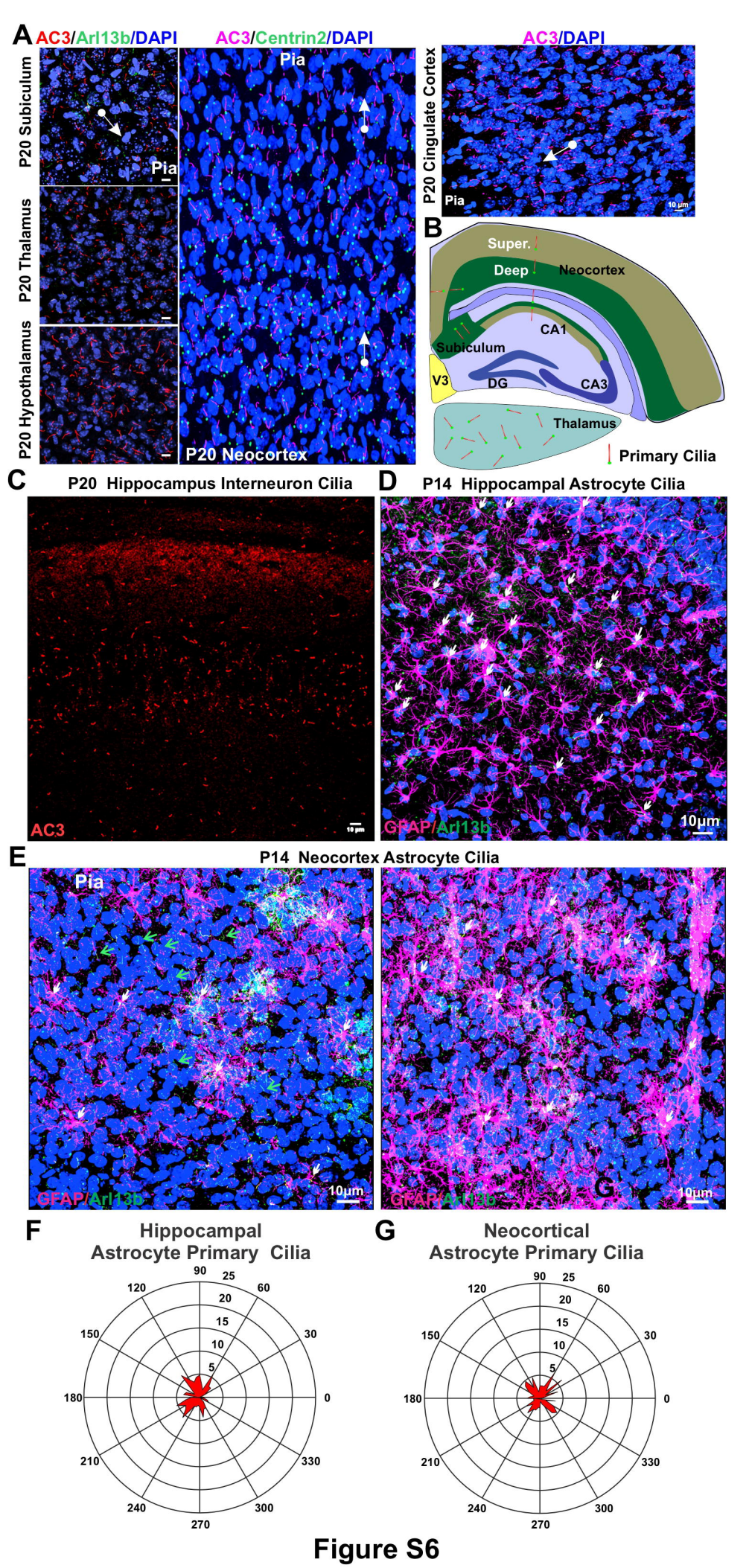
A
AC3/Arl13b/DAPI
AC3/Centrin2/DAPI
AC3/DAPI
P20 Subiculum
P20 Thalamus
P20 Hypothalamus
Pia
P20 Neocortex
P20 Cingulate Cortex
B
Super.
Deep
Neocortex
CA1
Subiculum
V3
DG
CA3
Thalamus
Primary Cilia
C
P20 Hippocampus Interneuron Cilia
AC3
D
P14 Hippocampal Astrocyte Cilia
GFAP/Arl13b
10μm
E
P14 Neocortex Astrocyte Cilia
G
F
Hippocampal
Astrocyte Primary Cilia
G
Neocortical
Astrocyte Primary Cilia

Figure S6

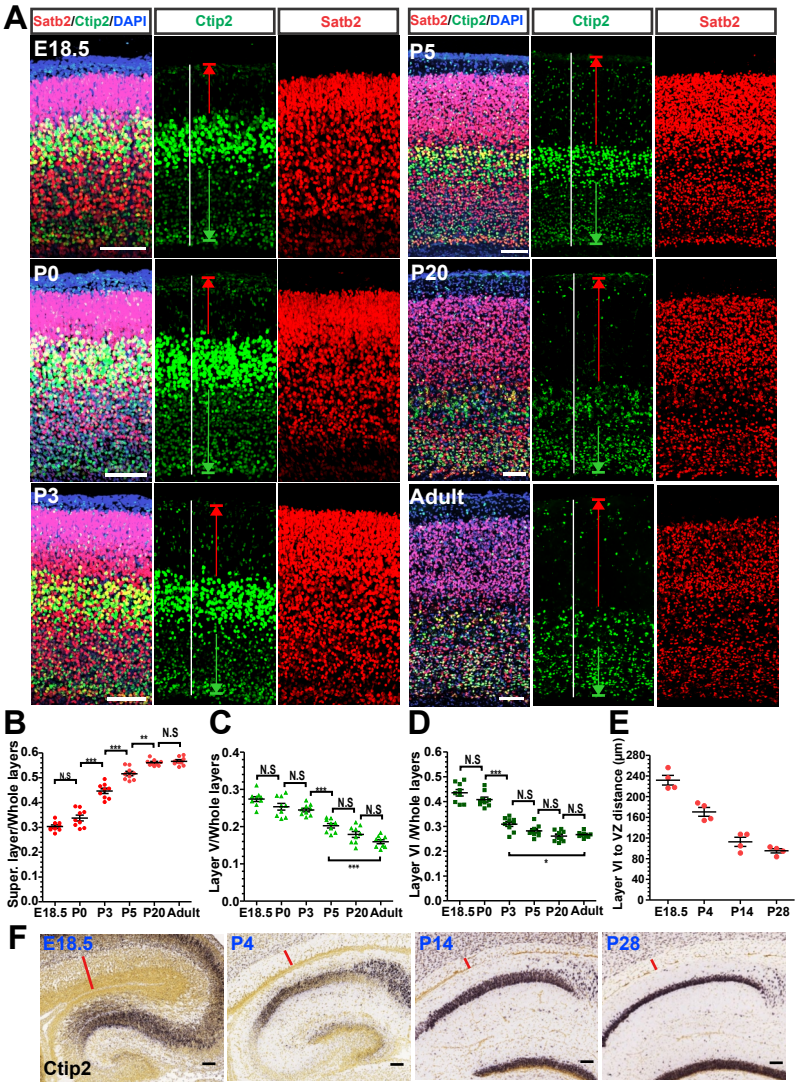
A
Satb2/Ctip2/DAPI
Ctip2
Satb2
E18.5
P5
P0
P20
P3
Adult
B
Super. layer/Whole layers
E18.5 P0 P3 P5 P20 Adult
C
Layer V/Whole layers
E18.5 P0 P3 P5 P20 Adult
D
Layer VI /Whole layers
E18.5 P0 P3 P5 P20 Adult
E
Layer VI to VZ distance (μm)
E18.5 P4 P14 P28
F
E18.5
P4
P14
P28
Ctip2

Figure S7

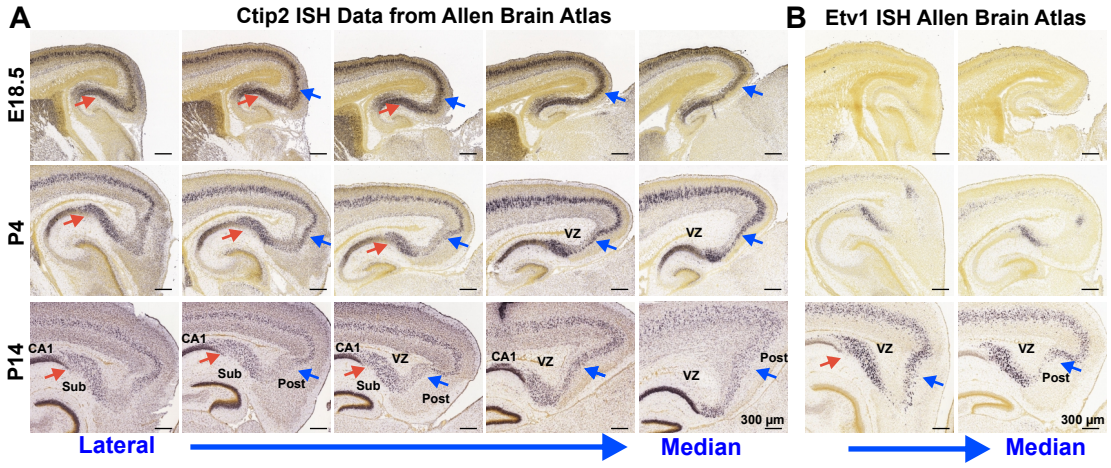
A
Ctip2 ISH Data from Allen Brain Atlas
B
Etv1 ISH Allen Brain Atlas
E18.5
P4
P14
CA1
Sub
Post
VZ
300 µm
Lateral
Median
Median

Figure S8

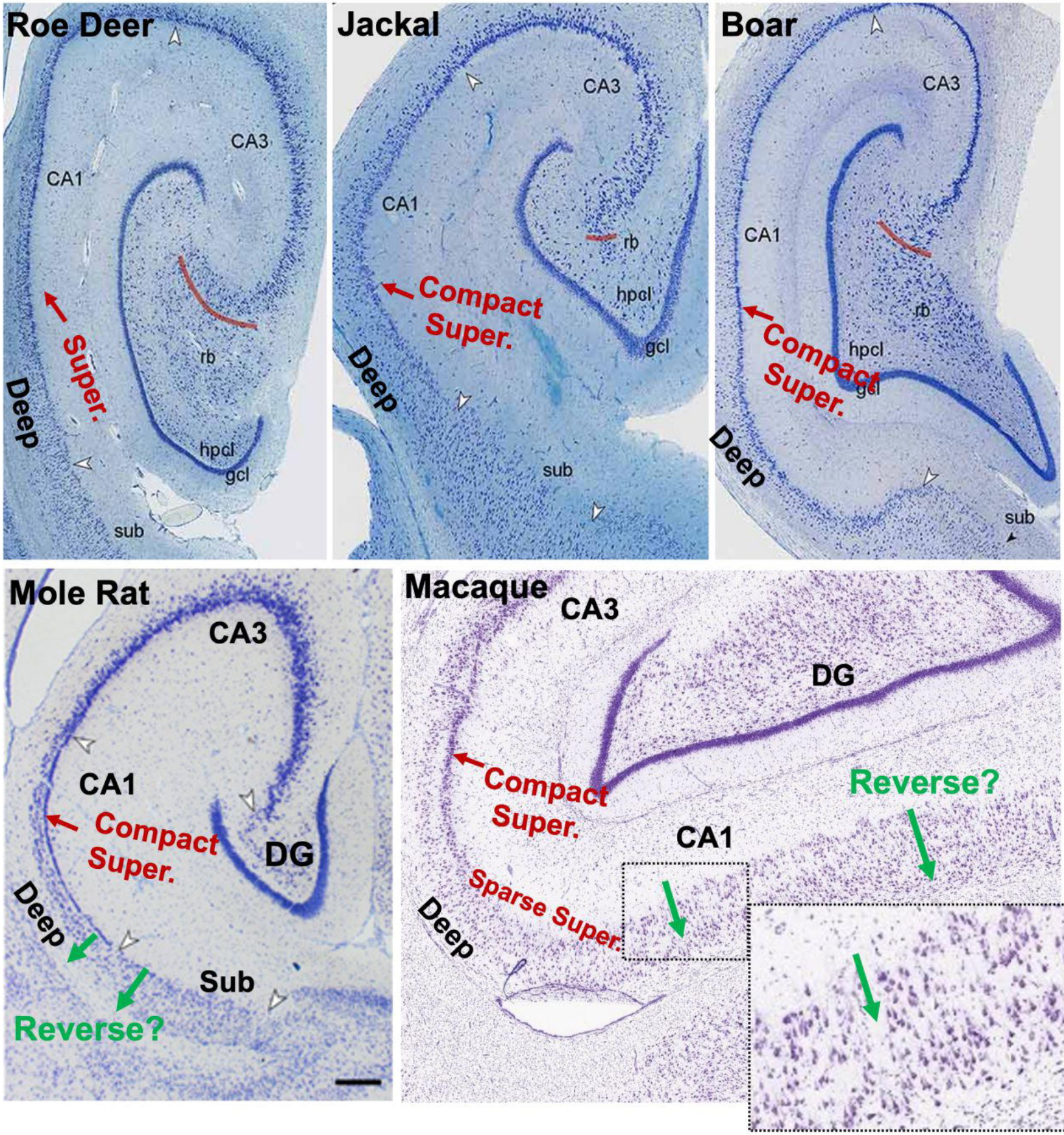
Roe Deer
CA3
CA1
Super.
Deep
rb
hpcl
gcl
sub
Jackal
CA3
CA1
Compact
Super.
Deep
rb
hpcl
gcl
sub
Boar
CA3
CA1
Compact
Super.
Deep
rb
hpcl
gcl
sub
Mole Rat
CA3
CA1
Compact
Super.
DG
Deep
Sub
Reverse?
Macaque
CA3
DG
Compact
Super.
Reverse?
CA1
Sparse Super.
Deep

Figure S9

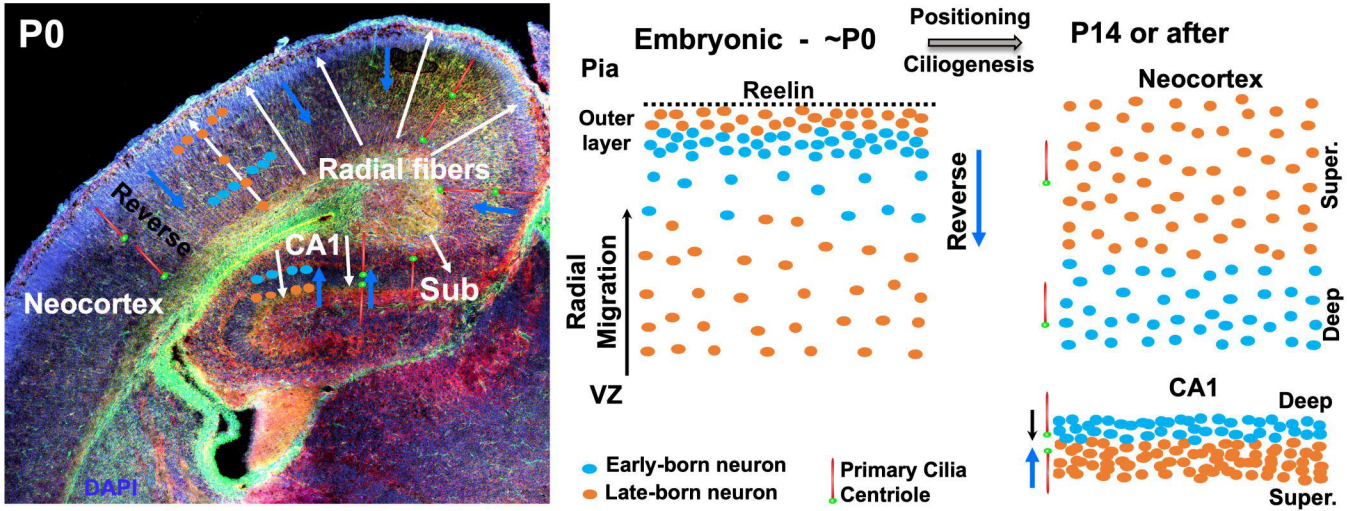
P0
Radial fibers
Reverse
CA1
Sub
Neocortex
DAPI
Embryonic - ~P0
Positioning
Ciliogenesis
P14 or after
Pia
Reelin
Outer layer
Reverse
Radial Migration
VZ
Neocortex
Super.
Deep
CA1
Deep
Super.
Early-born neuron
Late-born neuron
Primary Cilia
Centriole

Figure S10